Electrochemical Study of DNA Damage and Its Application for the Design of Carbon Nanomaterials based Combination Chemotherapy

by

Zhi Li

A thesis
presented to the University of Waterloo
in fulfillment of the
thesis requirement for the degree of
Master of Science
in
Chemistry (Nanotechnology)

Waterloo, Ontario, Canada, 2015

Author's Declaration

I hereby declare that I am the sole author of this thesis. This is a true copy of the thesis, including any required final revisions, as accepted by my examiners.

I understand that my thesis may be made electronically available to the public.

Abstract

Cis-diamminedichloroplatinum (II) (cisplatin or CDDP) is the first platinum based chemotherapy drug used for treating various types of cancers. It is discovered that the combination of cisplatin with electron donors can enhance the efficacy of the therapy, due to a unique electron transfer mechanism. Deoxyribonucleic acid (DNA) damage is a main step of the mechanism of this anticancer drug, which can be effectively detected by electrochemical methods. Carbon nanomaterials (CNMs) are electron-rich materials with abundant π electrons in their structure. With suitable functionalization, CNMs can become biocompatible and act as suitable electron donors to boost the cisplatin efficiency.

Here, we designed two electrochemical methods to detect DNA damage respectively using the redox signal of DNA bases, and an indicator species along with a single-stranded DNA modified gold electrode (ssDNA-AuE). In the first method, the oxidation signal of Deoxyguanosine monophosphate (dGMP) was characterized and chosen as an indicator for the study of DNA base damage. Decreased dGMP oxidation signal was observed after the dGMP was treated by cisplatin, which suggested the binding of cisplatin on guanine (G) base. However, when dGMP was treated by cisplatin in combination with N,N,N',N'-Tetramethyl-p-phenylenediamine (TMPD), no enhanced effect was observed probably due to the autoionization of TMPD in aqueous solutions. In the second method, the ssDNA-AuE was prepared through gold (Au)-thiol chemistry, and characterized using a redox pair, ferricyanide/ferrocyanide ($[Fe(CN)_6]^{3-}$/$[Fe(CN)_6]^{4-}$). Lower current response of $[Fe(CN)_6]^{3-}$/$[Fe(CN)_6]^{4-}$ was

observed at the ssDNA-AuE compared with the bare Au electrode, due to the repulsive force between this redox pair and the DNA strands on the electrode surface. After the ssDNA-AuE was treated by either cisplatin alone or cisplatin in combination with TMPD, the redox signal of $[Fe(CN)_6]^{3-}/[Fe(CN)_6]^{4-}$ increased at the treated ssDNA-AuE, indicating the interaction between DNA strand and cisplatin. We also discovered that both cisplatin binding and DNA strands break contributed to the recovered $[Fe(CN)_6]^{3-}/[Fe(CN)_6]^{4-}$ signal using elementary analysis. In addition, stronger $[Fe(CN)_6]^{3-}/[Fe(CN)_6]^{4-}$ signal was recovered on the ssDNA-AuE treated by the combination of cisplatin and TMPD than that treated by cisplatin only, showing that this method is sensitive enough to detect the enhanced effect caused by electron donors.

After the establishment of the detection methods, they was applied to monitor the combination effect of cisplatin and CNMs. Briefly, reduced graphene oxide (rGO) was synthesized through the modified Hummer's method followed by hydrazine reduction. After grafting Polyethylene glycol (PEG) on the rGO structure, the effect of PEG-rGO on the interaction of cisplatin and DNA was studied using the two designed electrochemical methods in this project and Clonogenic assay. However, all results show that the PEG-rGO has no noticeable effect on improving cisplatin efficiency. Therefore future work is needed to design an effective graphene based electron donor.

Our work suggests that the electrochemical method is a powerful tool for studying DNA damage, and can be applied to study the cisplatin and DNA interaction.

.

Acknowledgements

First of all, I would like to express my sincerest gratitude to my supervisors, Dr. Shirley Tang, and Dr. Qingbin Lu for their continuous support of my MSc study and research, for their patience, motivation, enthusiasm, and immense knowledge. Their guidance helped me in all the time of research and writing of this thesis.

Besides my supervisors, I would like to thank the rest of my thesis committee: Dr. Xiaosong Wang and Dr. Dayan Ban for their encouragement, insightful comments, and assistance.

Finally, I would like to thank past and present members of Dr. Shirley Tang's research group including Dr. David Donkor, Dr. Samaneh Shadmehr, Louis Cheung, Xiguang Gao, Kai Wang, Andrew Ward, Gaganprit Gill and Yun Wu.

Table of contents

List of figures

List of Abbreviations

$[Fe(CN)_6]^{3-}$/$[Fe(CN)_6]^{4-}$: Ferricyanide/ferrocyanide

△Ep: Redox peaks potential difference

A: Adenine

AFM: Atomic force microscopy

AMP: Adenosine monophosphate

Au: Gold

C: Cytosine

Cisplatin or CDDP: *Cis*-diamminedichloroplatinum (II)

CMP: Cytosine monophosphate

CNMs: Carbon nanomaterials

CNTs: Carbon nanotubes

CV: Cyclic voltammetry

DGGE: Denaturing gradient gel electrophoresis

dGMP: Deoxyguanosine monophosphate

DNA: Deoxyribonucleic acid

DPV: Differential pulse voltammetry

EDC: N-(3-dimethylaminopropyl-N'-ethylcarbodiimide) hydrochloride

EG: Epitaxial graphene

FT-IR: Fourier transform infrared spectroscopy

GC: Gas chromatography

GMP: Guanosine monophosphate

GO: Graphene oxide

HOMO: Highest occupied molecular orbital

IPA: Isopropanol

I_{pc}: Oxidation peak current intensity

LC: Liquid chromatography

LUMO: Lowest unoccupied molecular orbital

MCH: 6-Mercapto-1-hexanol

MES: (N-morpholino)ethanesulfonic acid

MS: Mass spectrometry

NHS: N-Hydroxysuccinimide

PEG: Polyethylene glycol

PEG-rGO: PEGylated reduced graphene oxide

PFGE: Pulsed field gel electrophoresis

Pt NPs: Pt nanoparticles

Pt: Platinum

SCGE: Single cell electrophoresis technique

SsDNA-AuE: Single-stranded DNA modified gold electrode

T: Thymine

TCNE: Tetracyanoethylene

TMP: Thymidine monophosphate

TMPD: N,N,N',N'-Tetramethyl-p-phenylenediamine

TUNEL assay: Terminal deoxyribonucleotidyl transferase mediated deoxyuridine

triphosphate nick End labeling

U: Uracil

UV-vis: Ultraviolet–visible

XPS: X-ray photoelectron spectroscopy

Chapter 1
Introduction

Cis-diamminedichloroplatinum (II) (cisplatin or CDDP) is the first platinum based chemotherapy drug used for treating various types of cancers[1–3]. However, the treatment based on cisplatin is limited by the serious side effects and cell resistance[4,5]. To circumvent the drawbacks of cisplatin, over three thousands of cisplatin analogues were designed based on the traditional hydrolysis mechanism. However, only oxaliplatin and carboplatin was approved by FDA[6,7]. This fact suggests that there is another molecular mechanism governing the toxicity of cisplatin. Recently, it was discovered that the combination therapy of cisplatin with electron donors dramatically enhanced the cancer cell killing, compared with the treatment of cisplatin only[8,9]. This amazing discovery supported a new cisplatin cytotoxicity mechanism proposed recently[10] and opened a new gate for us to design better platinum based chemotherapy.

Carbon nanomaterials (CNMs) such as carbon nanotube (CNT), graphene and their derivatives are expected to exhibit strong electron donating capability due to the their similar unique electronic structure.[11,12]. After suitable functionalization, carbon nanomaterials can become biocompatible and gain the ability to target cancer cells, achieving the targeted killing effect[13].

Electrochemical study of nucleic acid is a booming area in the past two decades. The recent research on Deoxyribonucleic acid (DNA) electrochemical study suggests that the electrochemical method is a powerful tool for the detection of DNA damage[14,15].

1.1 Cisplatin

1.1.1 Hydrolysis mechanism of cisplatin

Hydrolysis of cisplatin is long believed the key activation process before the formation of the harmful cisplatin-DNA adducts[1]. Figure 1.1 shows that cisplatin can be intracellularly activated by the leaving of its single or double leaving groups, the chloride, then binding onto DNA and forming the DNA adduct, thereby killing the cells.

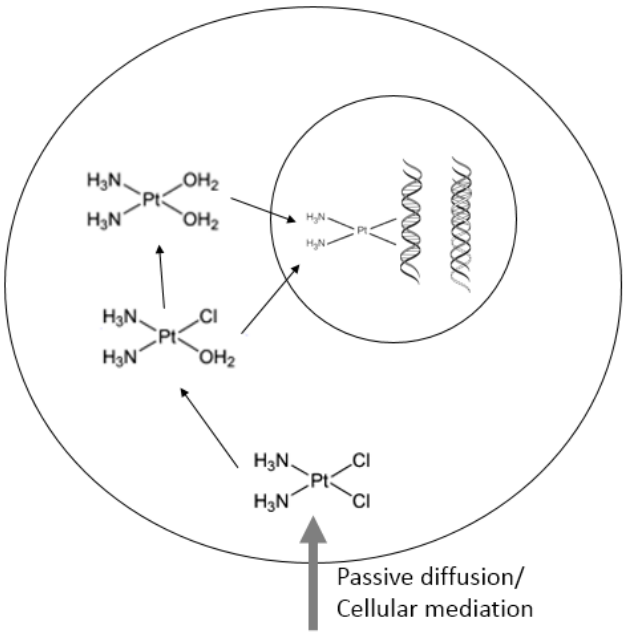

Figure 1.1: Scheme of hydrolysis of cisplatin.

Based on this mechanism, over three thousands of cisplatin analogues have been designed in order to relieve the side effects, such as nephrotoxicity, emetogenesis and neurotoxicity[16] and to broaden the treated cancer types. However, few of them entered the clinical trials and only oxaliplatin and carboplatin were approved by FDA[6,7]. So this discouraging fact suggests that there might be another molecular mechanism governing the toxicity of cisplatin. And that is the electron transfer mechanism.

1.1.2 Electron transfer mechanism of cisplatin

Recently, Lu and his coworkers discovered that the combination of cisplatin and an electron donor dramatically improved the efficiency of cisplatin[8,9]. This cheering discovery is based on a unique electron transfer mechanism observed by the femtosecond time-resolved laser spectroscopy[10].

This unique electron transfer mechanism can be expressed by the following reaction equations:

$$X + PtCl_2(NH_3)_2 = [PtCl_2(NH_3)_2]^{*-} + X^+ = X^+ + Pt(NH)_2Cl + Cl^- \quad (1.1)$$

$$X + Pt(NH)_2Cl \cdot = [PtCl(NH_3)_2]^{*-} + X^+ = X^+ + Pt(NH)_2 \cdot + Cl^- \quad (1.2)$$

$$X = G > A >> C, T$$

Instead of undergoing a hydrolysis process, cisplatin gains an electron directly from DNA bases (especially guanine (G)), forming an excited cisplatin star which quickly dissociate into a cisplatin radical and a chloride anion. This radical with one free electron is super reactive with another DNA base, leading to the leaving of the other chloride and the binding of $Pt(NH)_2$: to DNA bases.

The electron transfer mechanism not only supplied a new understanding of the molecular mechanism of cisplatin, but also unraveled the long existed mystery why cisplatin prefer to bind on two neighboring G bases, which has the highest electron donating capability among the four types of DNA bases.

1.1.3 Electron transfer mechanism based cisplatin combination chemotherapy

Based on the electron transfer mechanism, Lu and his coworkers predicted that combining a biological electron donor with cisplatin can greatly enhance the chemotherapeutic efficacy of cisplatin. So a combination therapy using N,N,N',N'-Tetramethyl-p-phenylenediamine (TMPD), a well-known electron donor due to its aromatic amines structure, and cisplatin was designed[9]. In the combination therapy of cisplatin and TMPD, the following reaction is expected to take place:

$$TMPD + CDDP \rightarrow TMPD^{+}: Cl^{-} + Pt(NH_3)_2CI \cdot \qquad (1.3)$$

Briefly, the TMPD molecule can act as an electron donor to give one electron to cisplatin, thereby forming the super reactive cisplatin radical, which can lead to the DNA strand breaks and therefore cell death.

In order to verify the electron transfer reaction between TMPD and cisplatin, fluorescence and Ultraviolet–visible (UV-vis) absorption spectroscopic measurements were performed. For both measurements, the characteristic signal belonging to $TMPD^{+}$ was observed, suggesting the occurrence of the electron transfer reaction.

In addition, DNA damage assay were carried out to study the actual efficacy of this type of combination therapy. In the gel electrophoresis assay, it is shown that cisplatin can directly induce DNA double strand break and the combination of cisplatin and TMPD greatly increased the yield of this kind of break by a factor of 3.5. This result provided a strong evidence that the radical produced in the dissociative electron transfer reaction shown in Eq. 3.1 greatly enhanced the DNA double strand break.

What is even more interesting is that this type of combination chemotherapy not only improved the cell killing, but also overcame the resistance of cisplatin-resistant cell lines, such as NIH:OVCAR-3 cells. NIH:OVCAR-3 is a cell line with high cisplatin resistance, showing a 40% cell viability percentage even after 250 uM cisplatin treatment for 24 hours. However, almost 90% cell killing was achieved by combining 100 uM TMPD and 100 uM cisplatin to treat the cells for 24 hours. And almost 100% NIH:OVCAR-3 cells were killed, when the concentration of cisplatin reached 150 uM.

In conclusion, this electron transfer mechanism based combination chemotherapy opened a new gate to design the platinum based chemotherapy, and provided a great opportunity to improve the treatment of many types of cancers.

1.2 Carbon nanomaterials

CNMs, including fullerene, carbon nanotubes (CNTs) and graphene, have attracted broad attentions due to their unique physical and chemical properties[17]. Figure 1.2 shows the structures of these three basic carbon nanomaterials.

As the fundamental structure of all the carbon nanomaterials, graphene became the most popular material since the first day it was discovered.

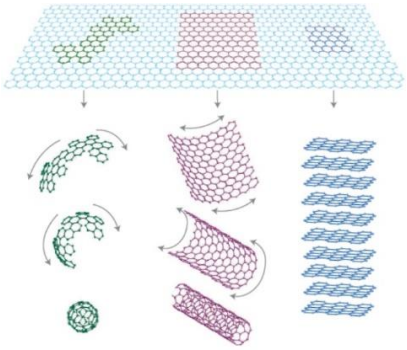

Figure 1.2: Structures of fullerene, carbon nanotube and graphene from left to right respectively.

1.2.1 Electron donating capability of graphene.

Graphene is a carbon allotrope made of bonded carbon atoms organized into a planer hexagonal lattice. The hybridization type of carbon in graphene is sp2, leaving an electron in the unhybridized p orbital to form a delocalized π (pi) bond. As a result, graphene has very unique electronic property and has the potential to act as either an electron donor or an acceptor[11,12].

Graphene is a unique zero band gap semiconductor due to the touch of its conduct and valence band at the Brillouin zone corners. The electron transfer between graphene and other molecules depends on the difference in the electronic chemical potential between them[18]. Briefly, whether graphene is an acceptor or donor is determined by the relative positions of graphene's Fermi level and the highest occupied molecular orbital (HOMO) and the lowest unoccupied molecular orbital (LUMO) of the interactant. Figure 1.3 shows when the LUMO of an interactant has lower energy level compared with the Fermi level of graphene, the electron will transfer from graphene to the interactant and forming a p-type doping, while the electron will transfer from the interactant to graphene when the interactant's HOMO energy is higher than the Fermi level of graphene.

The electron transfer between graphene and other molecules has been well studied by the surface doping of graphene[19–21]. It was reported that NO_2 can greatly decrease the resistance of graphene due to the electron transfer between graphene and NO_2[22]. The electron affinity of NO_2 is calculated to be about 0.4 eV below the Fermi level of graphene, determining that NO_2 is a very strong electron acceptor when interacting with

graphene. As a result, a high density of electrons is transferred from graphene to NO_2, leaving the graphene as a p-doped semiconductor with low resistance.

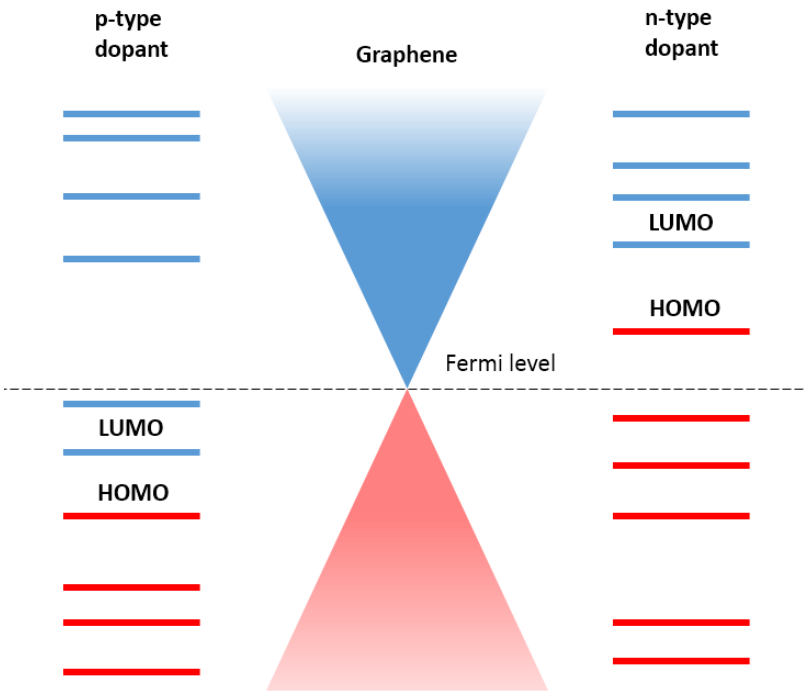

Figure 1.3: The scheme of the relative position of graphene's Fermi level and the LUMO and HOMO energy level of interactants.

Molecules with electron-withdrawing groups can also have electron transfer reaction with graphene. Rao *et al.* reported that nitrobenzene and tetracyanoethylene (TCNE) successfully produced the p-doping graphene evidenced by Raman spectra[23–26]. Chen *et al.* demonstrated that, by using synchrotron-based high-resolution photoemission spectroscopy, the electron transfer from epitaxial graphene (EG) to Tetrafluoro-tetracyanoquinodimethane was observed[21].

Even though the electron transfer reaction between cisplatin and graphene has never been studied, the interaction between graphene and platinum (Pt) was studied

before. Giovannetti *et al*. showed, by using density functional theory, that electrons transferred from graphene to Pt due to the difference in graphene' fermi level and Pt's electron affinity[27]. Considering the valence of Pt in cisplatin is 2^+, it is reasonable to expect that electrons transfer from graphene to this long-lived drug.

1.2.2 Synthesis of graphene

The common used synthesis method of graphene is the exfoliation and cleavage of graphite or thermal chemical vapor deposition[28–31]. The modified Hummer's method is an efficient way to produce graphene oxide (GO) through exfoliation and sonication. The GO synthesized through this method has very good solubility in water and some other solvents. Due to its low cost, convenience, high productivity and some other advantages, the modified Hummer's method is the most commonly used method to get graphene in research labs. Figure 1.4 shows how the GO is synthesized from graphite step by step through the modified Hummer's method.

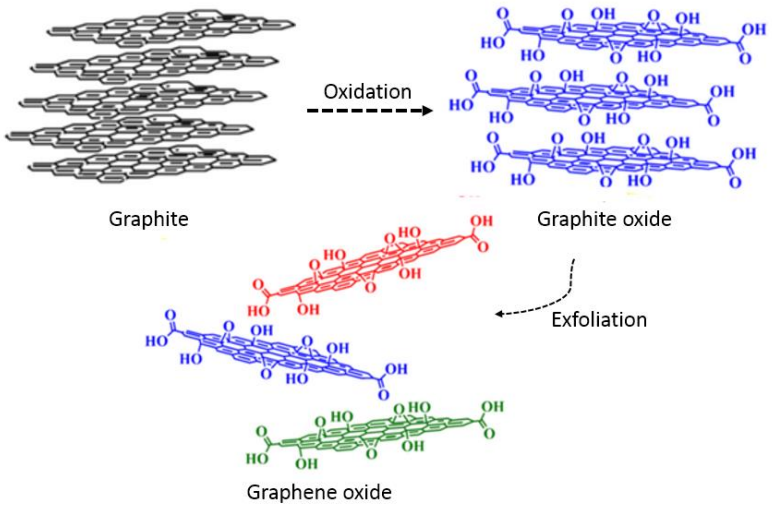

Figure 1.4: scheme of the modified Hummer's method for synthesizing GO.

However, the electronic property of graphene is damaged by the high density of

defects caused during the harsh oxidation process. So reduction treatments are usually needed, in order to recover the unique structure of graphene.

The main GO reduction strategies include thermal reduction and chemical reduction[32–35]. It was reported that GO can be reduced at high temperature, namely thermal annealing reduction[35]. However this reduction strategy is not suitable to be used for liquid sample because of the high temperature needed, potentially causing extra inconvenience to our future electron transfer test, so chemical reduction could be a better alternative for this project.

Usually, chemical reduction can be realized under some moderate environment, such as at room temperature. It makes the reduction in aqueous solution possible. Stankovich *et al.* initiated an easy chemical reduction method for GO using hydrazine[33,34]. The success of the reduction was confirmed by the C/O ratio in the structure and Raman spectroscopy. However the aggregation of graphene nanosheets was observed after the reduction by hydrazine or its derivatives. This irreversible aggregation after reduction restricted the application of graphene in many areas, such as the biological area in this project.

So in order to make graphene suitable for biological application, the priority is improving the biocompatibility and solubility of graphene. Dan *et al.* demonstrated that graphene can disperse well in water by controlling the hydrazine reduction conditions[36]. In their method, the hydroxyl and epoxy groups, but not carboxylic acid groups on the GO will be reduced by hydrazine under the conditions they described. Due to the electrostatic interaction between the negative charges on carboxylic acid groups, the

graphene nanosheets can disperse well in water without aggregation. However, the stability of this type of rGO is still not enough for biological application, because the high salt condition can disrupt the electrostatic interaction, and cause the aggregation again. As a result, further functionalization to the rGO is still necessary.

1.2.3 Functionalization of graphene

The main purposes of the functionalization in this project include improving graphene's biocompatibility and solubility as well as modifying graphene into a suitable electron donor. Until now, the most popular functionalization method to make graphene biocompatible is PEGylation[13,37–40].

The following are several properties of Polyethylene glycol (PEG) making it especially eligible in various biological and pharmaceutical applications

- Non-toxic and non-immunogenic – greatly enhance the biocompatibility of the functionalized molecules without interfering with cellular functions.
- Hydrophilic (aqueous-soluble) – PEGylation endows the functionalized molecules with perfect water solubility.
- Highly flexible – provides for surface treatment or bioconjugation without steric hindrance

The main strategies to link PEG on graphene include covalent method and non-covalent method[41]. Non-covalent method usually links PEG on graphene by the hydrophobic interaction. For example, graphene can be functionalized by phospholipid-PEG. For covalent method, a covalent bond is usually formed between PEG and graphene. The covalent method usually adopts conventional carbodiimide chemistry to

form the covalent bond. Zhuang *et al.* reported that amine-terminated branched PEG (six armed-PEG-NH_2) can be covalently conjugated on the carboxyl groups on GO surface under the help of N-(3-dimethylaminopropyl-N'-ethylcarbodiimide) hydrochloride (EDC)[41]. Michael *et al.* demonstrated that amine terminated linear PEG can be successfully grafted on GO using EDC-NHS as the catalyst[42].

Considering that the appearance of carboxyl groups and amine groups is the only demand for carbodiimide chemistry, the rGO prepared in Dan's protocol turns out to be a very suitable starting material for later PEGylation, because the electronic property was recovered and the required carboxyl groups was kept at the same time. Therefore this modified hydrazine reduction method together with the covalent PEG functionalization provides a suitable approach to produce a type of biocompatible reduced graphene for the study of the electron transfer reaction between graphene and cisplatin.

1.3 DNA damage study

Because DNA is the molecule which carries most genetic information in all living organisms, its integrity and stability is very important. However, DNA is sensitive to many factors and can be damaged because of either intrinsic or extrinsic reasons, leading to mutations and diseases like cancer. Detection of damage has important application in lots of areas such as theranostics, biosensor, targeted drug delivery and biomedicine. So developing economic and effective technique to detect DNA damage is necessary. The following content will briefly introduce several common DNA damage detection methods and the relatively new electrochemical method.

1.3.1 Common DNA damage detection methods

Electrophoresis: gel electrophoresis is a routine technique to identify, quantify and purify nucleic acid fragments[43,44]. Due to the negatively charged phosphate backbone in DNA structure, nucleic acid molecules can be moved by applying electric field through a matrix of agarose or other substances. For DNA fragment, the larger the size is, the more slowly it can move through the matrix, while the smaller the size is, the faster the fragment can move. As a result, the information about DNA structure change can be confirmed based on the position of DNA fragments in the gel. In the past decades, some improvements were made to gel electrophoresis technique, such as Single cell electrophoresis (SCGE)[45], pulsed field gel electrophoresis (PFGE)[46], Denaturing gradient gel electrophoresis (DGGE)[47], etc.

Although gel electrophoresis is relatively simple to perform and inexpensive, it does have some disadvantages such as poor sensitivity and low accuracy, as well as toxicity due to some DNA visualizing dyes such as Ethidium Bromide, which is a known carcinogen[48].

Mass spectrometry: the most outstanding feature of this technique is that MS can provide structural information about DNA damage. Coupled with gas chromatography (GC) or liquid chromatography (LC), some complex mixtures can be easily detected[49–51]. It was reported that, by using GC-MS technique, a variety of DNA damage products can be measured including sugar backbone, DNA bases and DNA-protein adducts[52]. Dizdaroglu demonstrated that a series of products from oxidatively damaged DNA bases could be measured by GC-MS successfully[53]. The quantification of DNA base

damage was achieved by adding stable isotope-labeled analogs of DNA bases as an internal standard[54]. However, artifacts may occur in this technique due to the high separating temperature. To reduce the artifacts, LC-MS technique was employed to detect the modified base products[55]. But the sensitivity of LC-MS is not as good as GC-MS. Considering the economy and efficiency, this technique is not an ideal method for DNA damage detection.

Terminal deoxyribonucleotidyl transferase mediated deoxyuridine triphosphate nick end labeling (TUNEL assay): Upon DNA fragmentation or breakage, the 3'-OH termini of DNA strands become free. This free termini will be catalytically labelled by dUTPs, which is secondarily labelled with markers such as a fluorophore, under the help from terminal deoxyribonucleotidyl transferase (TdT). Based on the signal from the marker, the DNA strand break can be detected and quantitated. Since Gavrieli *et al.* firstly reported this method in 1992, this method has been improved a lot to increase its accuracy[56,57]. The disadvantages of TUNEL assay include the tedious proceeding steps involved and the relatively high cost.

1.3.2 Electrochemical DNA damage study

The electrochemical study of DNA is a popular area in the past two decades[15]. According to statistics, an average of ~10 papers about DNA related electrochemical study were published per year between 1960~1989, while almost ~760 papers were published in 2010 alone. For the past few years, the number of publications about DNA related electrochemical study has been experiencing an exponential growth. So the electrochemical study of DNA will be a very popular and promising area in the future.

1.3.2.1 Electrochemistry of DNA bases

As early as seventy years ago, the electroactivity of adenine (A) has been shown through Polarographic reduction by Heath[58]. Further studies revealed both A and cytosine (C) and their nucleosides and nucleotides can be reduced with half-wave potentials at -1.33V for A and -1.44V for C (vs SCE)[59–62]. However, within the mercury electrode potential window, reduction of Uracil (U) and Thymine (T) was not observed. The reduction signal of G can only be observed when the potential almost reach the electrolyte discharge potential[63]. From these studies, it is shown that the reduction signal of most DNA bases was at very negative potential, and there was even no reduction of U and T within the mercury potential window. Along with the poisonous property of mercury, it turned out that using the reduction signal is not a convenient method to get DNA bases information.

For the oxidation of DNA bases, nucleotides, or nucleosides, carbon based electrodes are most frequently employed. Compared with Pyrimidine bases, Purine bases have lower oxidation potential, with G being the easiest one to be oxidized. Glenn *et al*. demonstrated, with a pyrolytic graphite electrode, that the oxidation of G went through a 4-electron process, with the –N(7)=C(8)H- bond oxidized initially and followed by the oxidation of the –C(4)=C(5)- bond, while the oxidation of adenine went through a 6-electron process with the similar initial step[64,65]. Oliveira *et al*. reported, at the glassy carbon electrode (GCE), that the oxidation peaks of G, A, T, C were characterized at +0.70 V, +0.96 V, +1.16V and +1.31V (vs Ag/AgCl) respectively[66]. Similar results were obtained by Stempkowska at the paste carbon electrode, showing

the oxidation peaks of Guanosine monophosphate (GMP), adenosine monophosphate (AMP), thymidine monophosphate (TMP) and cytosine monophosphate (CMP) at +1.00 V, +1.28 V, 1.47 V and 1.53 V (vs Ag/AgCl) respectively[67].

DNA base damage can be induced by oxidative agents, reductive agents and genotoxic agents. Currently, the DNA base damage is usually detected using optical method coupled with some separation techniques, such as liquid chromatography, making the detection laborious and expensive[68,69]. Alternatively electrochemical methods can be applied to detect base damage induced change in intrinsic redox signals such as the reduction of the oxidation peak. G is the most common target for a broad range of these base reactive agents, and also gives the easiest measurable signal at carbon based electrodes, making the electrochemical study of G and its nucleotide and nucleoside a feasible approach to study DNA base damage. Up to now, many base targeting agents have been studied using DNA base electrochemistry, such as hydrazine derivatives, Adriamycin and quercetin[70–72]. For platinum based genotoxic agents, Brabec successfully detected the G oxidation peak decrease by using differential pulse voltammetry (DPV) after treating DNA with a platinum based anticancer drug, $[Pt(dien)(H_2O)]^{2+}$, [73].

1.3.2.2 DNA modified electrode

The modification of electrode was studied as early as 20 years ago. Kelly *et al.* first reported that carbon glassy electrode can be modified by DNA oligonucleotides, and used for the detection of DNA hybridization[74]. After that, more DNA modified electrodes were designed for the study of DNA hybridization, DNA sequencing and

DNA damage[75–78]. Due to the stability and convenience of thiol-gold (Au) chemistry, DNA modified Au electrode are the most common choice at present[79,80].

DNA modified electrodes can be used for two types of measurements depending on the origin of the electrochemical signal. The first measures the intrinsic redox signal of DNA, for example, the oxidation signal of G. The second measures the redox signal of other indicators, such as methylene blue, ferrocene, hexaaminеruthenium ($[Ru(NH_3)_6]^{3+}$), etc.

It is well known that a DNA strand bears negative charges due to the phosphate groups in its structure. After attaching DNA strands to an electrode, the negatively charged electrode surface can be either repulsive or attractive towards negatively charged or positively charged redox indicators respectively. As a result, the concentration of the redox indicator at the surface of a DNA modified electrode will be different compared with that at a bare electrode, leading to different current response. Li *et al.* reported that DNA modified Au electrodes can pre-concentrate $[Ru(NH_3)_6]^{3+}$ at the electrode surface, giving higher current intensity compared with bare Au electrodes[81]. Miranda e*t al.* demonstrated that the negatively charged redox pair ferricyanide/ferrocyanide ($[Fe(CN)_6]^{3-}$/$[Fe(CN)_6]^{4-}$) gives lower redox current on a DNA modified electrode than that on a bare Au electrode in its CV curves[82].

Initially, DNA modified electrodes were mainly used for DNA hybridization detection. Later on, these devices were used for the detection of DNA damage including DNA strand break and single base mismatch. Labuda *et al.* demonstrated a method for the detection of DNA double strand disruption using redox species binding specifically

to double-stranded DNA and producing a redox signal at carbon electrodes[83–85]. Upon DNA degradation, the redox signal decreased because of its lower affinity to single-stranded DNA (ssDNA). Jacqueline *et al.* successfully monitored the kinetics of DNA restriction caused by a DNA restricting enzyme, R.PvuII, using the signal of some redox species linked on DNA strands[86]. When DNA was restricted by the enzyme, the redox species left the electrode surface and the redox signal were lost.

In summary, the electrochemical study of DNA is a very powerful tool to detect DNA damage. The advantage of electrochemical methods include low cost, high reliability, high speed and simplicity.

Chapter 2
Design of electrochemical detection methods for detecting the cisplatin and DNA interaction

2.1 Introduction

As it was mentioned in Chapter 1, cisplatin can undergo electron transfer reaction with DNA bases and therefore forming the cisplatin-DNA adducts. By adding biological electron donors, more DNA double strand break was found and the cell killing efficiency was enhanced. So we can utilize the intrinsic oxidation signal of G to study the interaction between cisplatin and DNA base. The reason we use G is that it has the highest reactivity to cisplatin among all DNA bases, and meanwhile has the lowest oxidation potential, effectively avoiding the high background current at high potential range. In addition, Au electrodes can be modified by ssDNA and the $[Fe(CN)_6]^{3-}/[Fe(CN)_6]^{4-}$ redox pair can be used as an indicator to show the interaction between cisplatin and the DNA strands on the electrode surface. Due to the electrostatic repulsion between ssDNA and this negatively charged redox pair, the intensity of the redox current is expected to decrease greatly after DNA modification. After the DNA strands on electrode surface was treated by cisplatin, both cisplatin binding and DNA strand break are expected to introduce changes to the redox current.

In this chapter, two electrochemical methods adopting intrinsic DNA redox signal and extrinsic species redox signal will be designed to monitor the DNA damage caused by cisplatin and the enhanced DNA damage caused by combining cisplatin and electron donors.

2.2 Electrochemistry of guanine

2.2.1 Introduction

The electrochemical study of G has been performed at carbon based electrodes, Au electrodes, platinum electrodes, mercury electrodes previously[64]. The most distinguishable signal is given by carbon based electrodes including pyrolytic graphite, glassy carbon, carbon paste and some other modified carbon electrodes. Most of these studies were done by the two most commonly used electrochemical methods, DPV and cyclic voltammetry (CV), and the later method is the one used in this project.

For CV, a three electrodes system, including working, reference electrode and counter electrodes[87], is used. A triangle shape potential is applied to the working electrode (as shown in Figure 2.1) and facilitate the electron transfer between the redox species and the electrode surface. When the applied potential on working electrode is more positive than the standard potential of the redox species in solution, the relative species will be oxidized, thereby producing a cathodic current (electrons going from solution to electrode). Similarly, as the potential scans back, an anodic current will be produced (electrons going from electrode to solution).

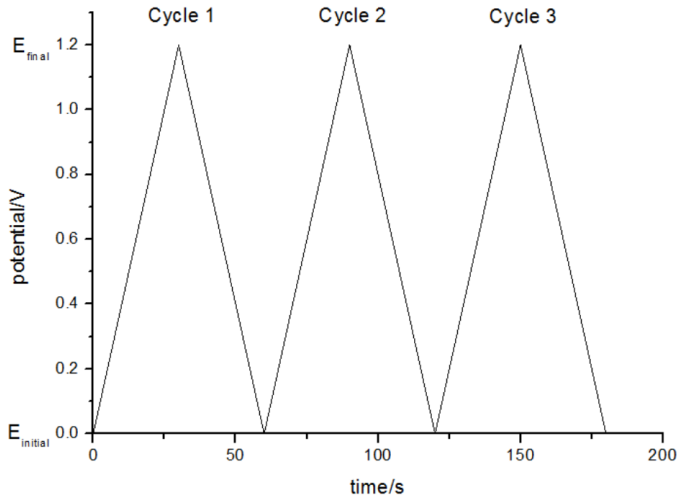

Figure 2.1. A CV potential waveform with switching potentials.

By IUPAC convention, anodic currents are positive and cathodic currents negative, so a typical CV curve of a reversible reaction looks like the one shown in Figure 2.2a. For an irreversible electrochemical reaction, due to the slow charge transfer or unstable electrochemically produced products, the CV curve looks like the one shown in Figure 2.2b.

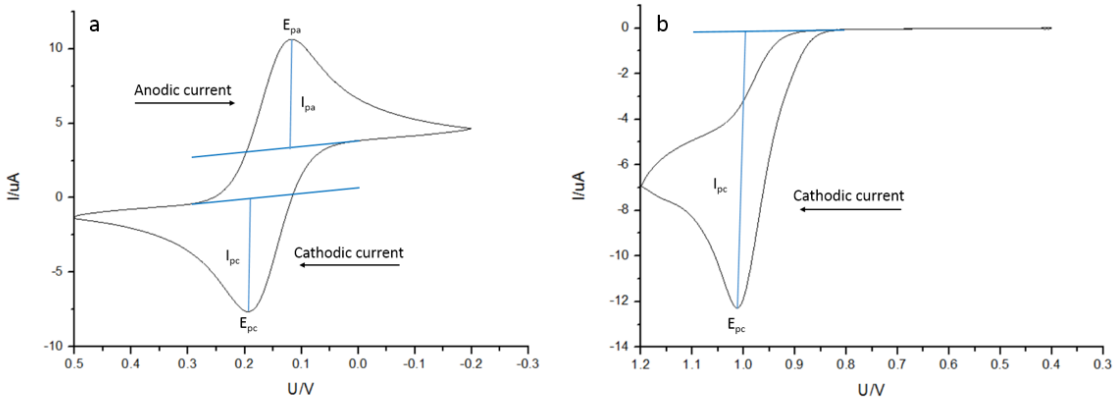

Figure 2.2: (a) Typical CV curve of a reversible electrochemical reaction. (b) Typical CV curve of an irreversible electrochemical reaction. In this case, the product after oxidation is unstable so there is only anodic current but not cathodic current.

In both situations, the peak current has a linear relationship with the analyte concentration as expressed in Equation 2.1a and 2.1b[87].

Reversible reaction: $\boldsymbol{i}_p = (2.69x10^5)n^{3/2}ACD^{1/2}v^{1/2}$ (2.1a)

Irreversible reaction: $\boldsymbol{i}_p = (2.99x10^5)n(\alpha na)^{1/2}ACD^{1/2}v^{1/2}$ (2.1b)

Where i_p is the peak current, n is the number of electrons transferred in the electrochemical reaction, A is the area of electrode, D is the diffusion coefficient of the species, v is the scan rate and C is the concentration of the redox species.

2.2.2 Materials and Methods

Chemicals and reagents: Deoxyguanosine monophosphate (dGMP) (D9500, MW: 347.22), cisplatin (P4394, MW: 300.05) and TMPD (T7394, MW: 164.25) were purchased from Sigma-Aldrich and used without further purification. 0.1 M stock dGMP solution and 4 mM stock cisplatin solutions were prepared using Milli-Q water. 0.1 M TMPD stock solution was prepared using HPLC degree ethanol (34852) purchased from Sigma-Aldrich.

Characterization of dGMP oxidation signal: a series of dGMP solutions with concentrations of 0 uM (as the background current) 100 uM, 300 uM, 500 uM and 1 mM were prepared by using the stock dGMP solution and 0.5 M pH 5.0 acetate buffer. Before tests, the GCE (CH Instruments, Inc. CHI104) was polished using1 um, 0.3 um and 0.05 um alumina in sequence (the electrode was rinsed carefully between each polish) and softly sonicated in a 30 % ethanol solution for 5 mins to clean the electrode surface. To improve the reproducibility, the polished GCE was electrochemically activated by being scanned in a 0.5 M H_2SO_4 solution from -0.5 V to 1.5 V at 0.1 V/s

scan rate until stable CV curves were obtained. CV curves of the prepared series of dGMP solutions were recorded using a CHI650 potentiostat through a three electrodes system (Figure 2.3a) including the as-treated GCE (working electrode), a Sliver/Sliver chloride (Ag/AgCl) (reference electrode) and a Pt wire electrode (counter electrode).

Interaction between cisplatin and DNA base: a mixture of 500 uM cisplatin and 500 uM dGMP solution was prepared by using the stock solutions and 0.5 M acetate buffer at pH 5.0. Pure 500 uM cisplatin solution was prepared by using the same stock cisplatin solution and acetate buffer, in order to test the background current. CV curves of both solutions after 0, 5, 10, 24 and 48 hours incubation at room temperature were recorded using the same electrodes and potentiostat mentioned before.

Effect of TMPD on interaction between cisplatin and DNA base: solutions of 500 uM dGMP and 1 mM TMPD mixed with 50, 100, 200, 300 and 500 uM cisplatin respectively were prepared by using the stock solutions and 0.5 M acetate buffer at pH 5.0. Solutions of 1 mM TMPD mixed with 50, 100, 200, 300 and 500 uM cisplatin respectively were prepared by using the same stock solutions and acetate buffer, in order to gain the background currents. CV curves of solutions with 500 uM cisplatin with and without TMPD were recorded after 0, 5, 10, 24 and 48 hours incubation using the same electrode and potentiostat mentioned before. CV curves of all the other solutions were recorded after 0 and 24 hours using the same electrode and potentiostat.

2.2.3 Results and Discussion

The CV curves of dGMP at different concentrations were shown in Figure 2.3b. Part of the oxidation signal of dGMP overlapped with the background current from the oxidation of water, causing problems to correctly identify the dGMP oxidation peak. The background-subtracted CV curves of dGMP at different concentrations were produced after subtracting the background current as shown in Figure 2.3c. It turned out that dGMP only had one oxidation peak around 1.1 V, but no reduction peak was observed, demonstrating that an irreversible reaction due to the unstable oxidized product, which is consistent with the previous literature[67]. In addition, a perfect linear relationship was found between the oxidation peak current intensity and the dGMP concentration as shown in Figure. 2.3d. In conclusion, the dGMP oxidation peak was successfully characterized by using the GCE and the CV method described in this project.

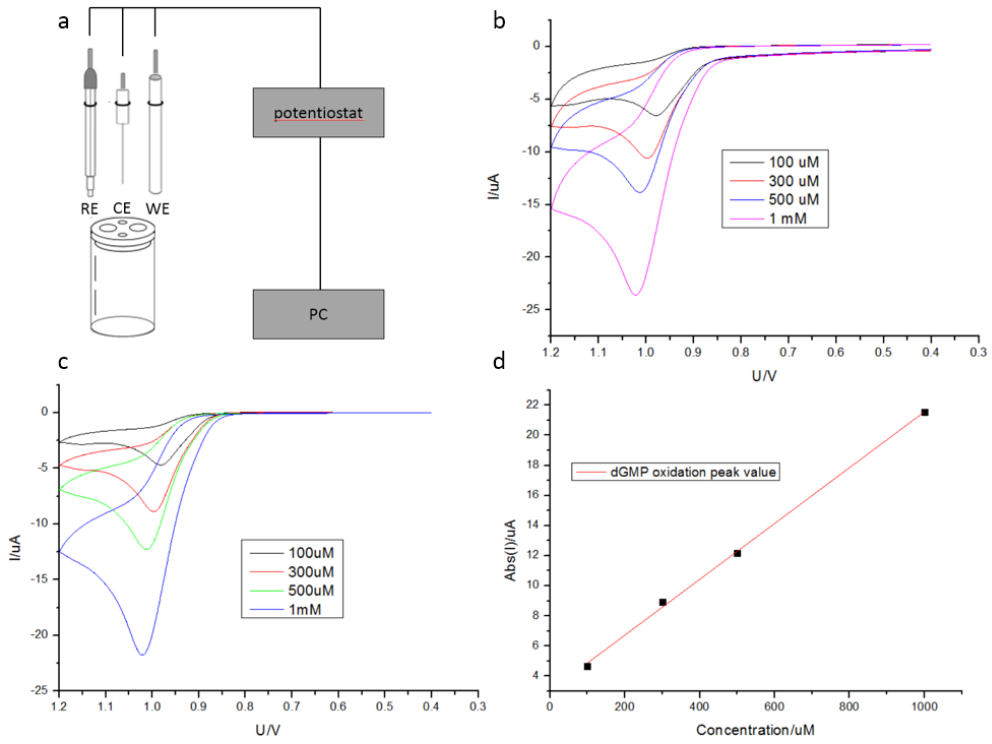

Figure 2.3: (a) The experiment setup for the electrochemical test. (b, c) CV of dGMP at different concentration before and after background subtraction. Scan rate: 20 mV/s (d) the absolute value of dGMP oxidation peak current versus dGMP concentration, the line is a linear fit of the data points.

Figure 2.4a shows the effect of cisplatin on dGMP oxidation signal. After 5 hours incubation, the absolute value of dGMP oxidation peak decreased from 10.42 to 9.614 uA. After 48 hours incubation, the absolute value of dGMP oxidation peak decreased to 5.2 uA, showing that over half of the dGMP signal was reduced by cisplatin. Brabec demonstrated that upon the binding of cisplatin on G base, the oxidation current will decrease to 80 times lower than the G base itself[73]. So the decrease of the dGMP oxidation signal in our experiment can be attributed to the binding of cisplatin on this G base containing nucleotide. By analyzing the degree of this oxidation peak decrease, the adduction of cisplatin on dGMP can be monitored.

Furthermore, the effect of the electron donor, TMPD, on the interaction between cisplatin and dGMP was tested, as shown in Figure 2.4 b. The CV curves of the solution containing 500 uM dGMP and 500 uM cisplatin plus 1mM TMPD at various time points showed similar decrease in current intensity. To show the effect of TMPD on dGMP damage induced by cisplatin, the dGMP oxidation peak values in both situations (with and without TMPD) versus incubation time was plotted, as shown in Figure 2.4c. However, TMPD only slightly increased the initial absolute value of dGMP oxidation peak from 10.42 uA to 12.04 uA rather than leading to a more dramatic decrease of dGMP oxidation peak. After normalization, the changes of normalized peak value over

time are almost identical regardless of the presence TMPD, (Figure 2.4d).

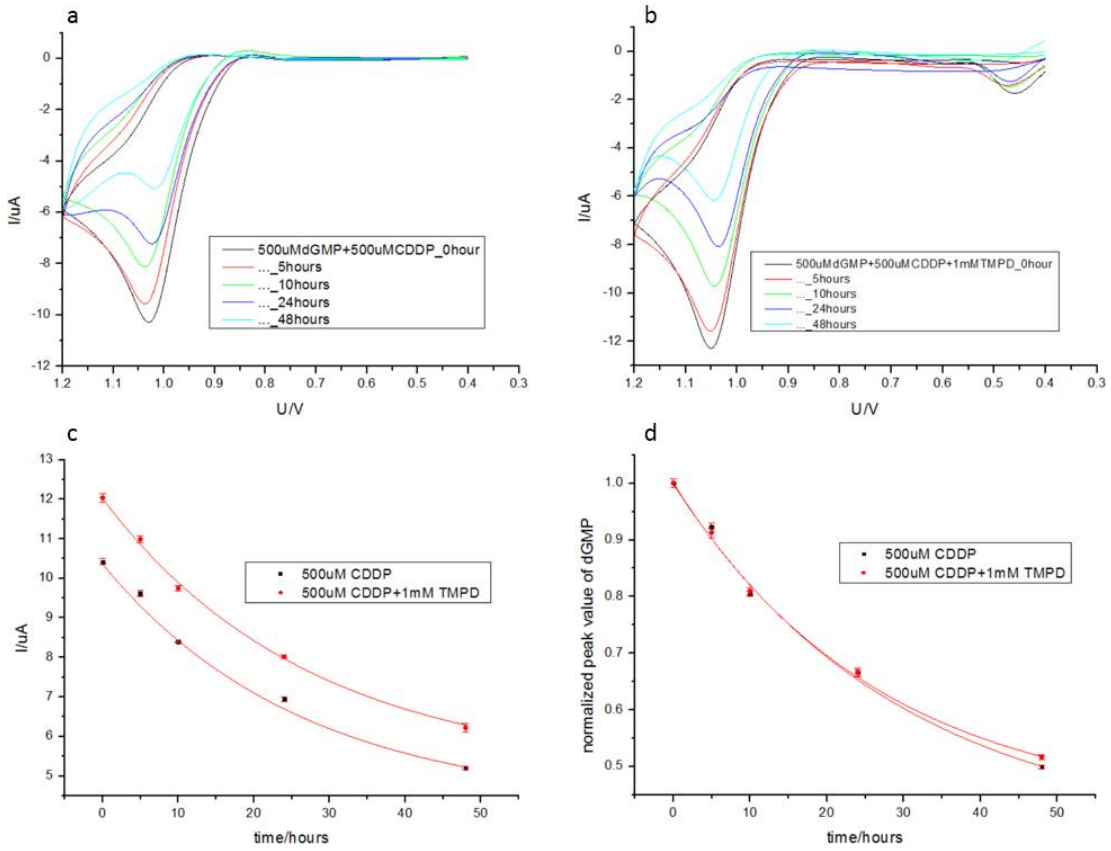

Figure 2.4. Background subtracted CV curves of dGMP mixed with (a) 500 uM CDDP and (b) 500 uM CDDP+1mM TMPD after 0,5,10, 24 and 48 hours, Scan rate: 20 mV/s (c) absolute and (d) normalized oxidation peak current intensities of 500 uM dGMP mixed with 500 uM CDDP (■), 500 uM CDDP+1 mM TMPD(●) over time.

Futhermore, 500 uM dGMP was mixed with a series of lower concentrations of cisplatin with and without TMPD and the CV curves of dGMP were recorded. Figure 2.5 shows the dGMP oxidation peak percentage value after 24 hours treatment by cisplatin only, and cisplatin in combination with TMPD. At all cisplatin concentrations, TMPD didn't show any noticeable effect.

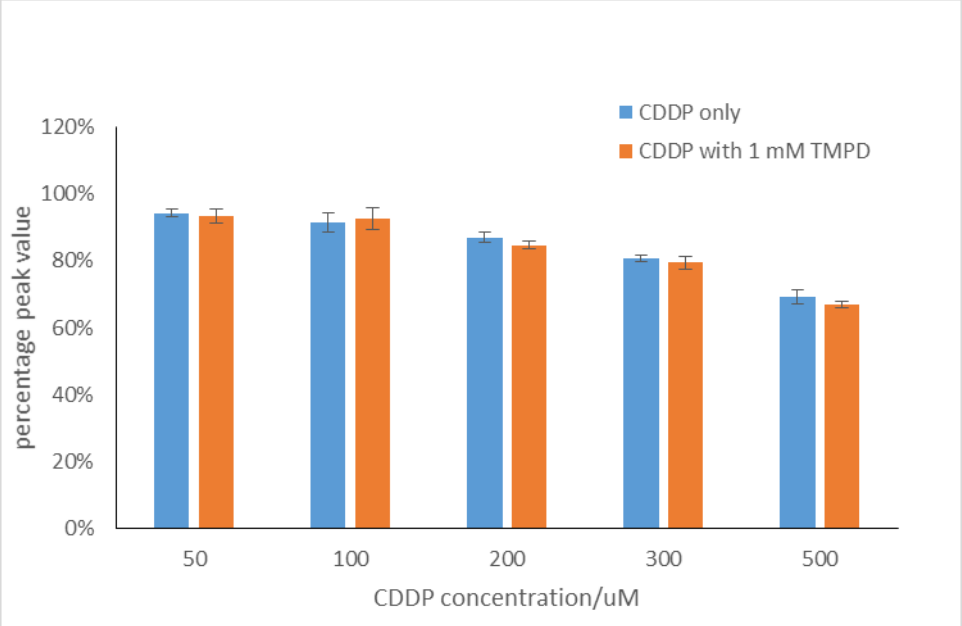

Figure 2.5: Percentage peak value of 500 uM dGMP mixed with various concentrations of CDDP only (■), various concentrations of CDDP in combination with 1 mM TMPD (■) after 24 hours reaction (the initial peak value is the peak value after 0 hours reaction). Scan rate: 20 mV/s

TMPD is a very reactive compound and reported to be autoionized easily even in water due to its low ionization potential[88,89]. In our experiment, the color change of the water solutions containing TMPD was also observed after a couple hours of incubation. This autoionization could be the reason why we didn't see the enhanced dGMP damage in this experiment. However, both the DNA strand break study and cell viability test conducted in Lu's work were also in water environment, and the enhanced effect caused by TMPD (same cisplatin/TMPD ratio as used in this project) was able to be observed in their experiments[9]. Therefore, further investigation is needed to confirm whether the autoionization of TMPD in water is the reason for the lack of enhanced cisplatin adduction on the G base observed in this set of experiment.

2.2.4 Conclusion

In summary, the dGMP oxidation peak was characterized and investigated, at GCE by using CV method. The interaction between dGMP and cisplatin was confirmed by the decrease of the dGMP oxidation peak current intensity at various time points. The effect of TMPD on the interaction between dGMP and cisplatin was investigated by incubating these three substances together. However, the combination of cisplatin and TMPD didn't lead to faster or more pronounced decrease in the dGMP oxidation peak compared with cisplatin itself. TMPD is known to undergo autoionization when interacting with water, even though enhanced DNA double strand break and cell killing efficiency were observed in aqueous solutions previously. Future experiments with alternate designs, for example, by using a non-aqueous electrolyte to avoid the autoionization of TMPD or using some other electron donors which are stable in water, might be needed to observe the combinational effects on DNA damage.

2.3 DNA modified Au electrode for DNA damage study

2.3.1 Introduction

Au surfaces can be easily modified using thiol terminated compounds via the robust Au-sulfur bond. This Au modification strategy is used in many areas including surface science, biotechnology, inorganic chemistry, and has potential applications in biosensor, drug delivery, Au nanoparticle modification, etc[90–92]. Therefore, thiol terminated DNA strand can be a feasible approach to make the DNA modified Au electrode. The success of the modification can be verified by using electrochemical analysis and elementary analysis techniques such as X-ray photoelectron spectroscopy (XPS).

The interaction between cisplatin and DNA can be studied by the change in the redox signal of an electroactive pair $[Fe(CN)_6]^{3-}/[Fe(CN)_6]^{4-}$. As mentioned in Chapter 1, repulsive force exists between the DNA modified electrode surface and the $[Fe(CN)_6]^{3-}/[Fe(CN)_6]^{4-}$ redox pair because of the negatively charged DNA phosphate backbone. After treated by cisplatin, the DNA strands on the electrode could be damaged, so the $[Fe(CN)_6]^{3-}/[Fe(CN)_6]^{4-}$ indicator would give different response. Based on the change of $[Fe(CN)_6]^{3-}/[Fe(CN)_6]^{4-}$ signal, the interaction between cisplatin and DNA can be studied.

2.3.2 Materials and Methods

Chemicals and reagents: DNA oligomer was purchased from Integrated DNA Technologies. The DNA sequence is 5'-SH-AAAAAAAAACCCAGGTTCTCT. DNA

stock solution of 100 uM was prepared and stored at 20 ℃. 6-Mercapto-1-hexanol (MCH) was purchased from Sigma-Aldrich. MCH stock solution of 100 mM was prepared and stored at room temperature. $[Fe(CN)_6]^{3-}$ was obtained from J. T. Baker and a stock solution of 1 M was prepared.

Modification of Au electrode: Initially, the Au electrode (CH Instruments, Inc. CHI101) was treated with the piranha solution for 20 mins to remove the organic impurities, followed by rinsing with Milli-Q water. The treated electrode was polished afterwards by using 1 um, 0.3 um and 0.05 um alumina in sequence (the electrode was rinsed carefully between each polish) and gently sonicated in a 30 % ethanol solution for 5 mins. To improve the reproducibility, the clean electrode was electrochemically activated by being scanned in a 0.5 M H_2SO_4 solution from -0.5 V to 1.5 V at 0.1 V/s scan rate until stable CV curves were obtained. The as-prepared Au electrode was incubated in a 3 uM thiol terminated single-stranded DNA (ss-DNA) solution for 4 hours, followed by 1 hour 1 mM MCH treatment to remove the unstable linked DNA strands out of the electrode surface. The single-stranded modified gold electrode (ssDNA-AuE) was kept in water for future use.

Electrochemistry of ssDNA-AuE: the CV curves of 5 mM $[Fe(CN)_6]^{3-}/[Fe(CN)_6]^{4-}$ was recorded by using the bare Au electrode (after the standard cleaning process) and the ssDNA-AuE from -0.2 V to 0.6 V (vs Ag/AgCl) respectively, with a scan rate 0.01 V/s.

Study of the interaction cisplatin and DNA strand: 500 uM cisplatin solution was prepared by using the stock cisplatin and ethanol. The CV curves of 5 mM

$[Fe(CN)_6]^{3-}/[Fe(CN)_6]^{4-}$ was recorded under the same scan condition, by using the ssDNA-AuE after 0, 2, 4, 8 and 19 hours treatment in the 500 uM cisplatin solution.

Effect of TMPD on the interaction between cisplatin and DNA strand: 500 uM TMPD (as a control) and a mixture of 500 uM cisplatin and 1 mM TMPD solutions were prepared by using the stock solutions and ethanol. The CV curves of 5 mM $[Fe(CN)_6]^{3-}/[Fe(CN)_6]^{4-}$ was recorded under same scan condition, by using the ssDNA-AuE after 0, 2, 4, 8 and 19 hours treatment in the prepared solutions.

Elementary analysis of the DNA modified Au surface: a piece of Au coated silicon wafer was prepared (a gift from Prof. Jonathan Baugh's lab) and used for further DNA modification. The prepared Au surface was rinsed with acetone, isopropanol (IPA) and Milli-Q water in sequence and blown dried by pure nitrogen gas. The as-treated Au surface was modified by using 3 uM thiol terminated ssDNA solution to make the DNA modified Au surface. Half of the Au coated silicon wafter was incubated in a 500 uM cisplatin solution for 8 hours and rinsed with Milli-Q water for XPS characterization. All XPS spectra were acquired by using a Thermo Scientific ESCALAB 250Xi XPS spectrometer with a monochromatic Al-Kα X-ray source. High resolution scans were acquired for N 1s, P 2p, Au 4f and Pt 4f regions for the DNA functionalized on the Au coated silicon wafer. All XPS spectra were analyzed by using the software CasaXPS.

2.3.3 Results and Discussion

CV curves of 5 mM $[Fe(CN)_6]^{3-}/[Fe(CN)_6]^{4-}$ were recorded by using the bare Au electrode and the ssDNA-AuE respectively (Figure 2.6a). From the CV curve gained at bare Au electrode, a reversible reaction, with a redox peaks potential difference (△Ep)

74 mV and a oxidation peak current intensity (I_{pc}) -10.45 uA, was confirmed. Upon the modification of DNA on the electrode, the I_{pc} of $[Fe(CN)_6]^{3-}/[Fe(CN)_6]^{4-}$ greatly decreased to -0.6429 uA along with the separation of the △Ep to 499 mV. It is as expected because the repulsive force between the DNA strands on the electrode surface and $[Fe(CN)_6]^{3-}/[Fe(CN)_6]^{4-}$ pushed the anions away and slowed down the electron transfer rate between the two interfaces. So a lower current response of $[Fe(CN)_6]^{3-}/[Fe(CN)_6]^{4-}$ was observed. Based on this change, the ssDNA-AuE was characterized.

Figure 2.6b shows the CV curves of $[Fe(CN)_6]^{3-}/[Fe(CN)_6]^{4-}$ tested on the ssDNA-AuE treated by cisplatin only and that treated by cisplatin in combination with TMPD after 8 hours. For cisplatin only, the CV curve of $[Fe(CN)_6]^{3-}/[Fe(CN)_6]^{4-}$ shows that the I_{pc} recovered from -0.6364 uA to -6.106 uA and the △Ep decreased from 499 mV to 221 mV, indicating that cisplatin partly reduced the repulsive interaction between DNA strands and $[Fe(CN)_6]^{3-}/[Fe(CN)_6]^{4-}$. For the combination of cisplatin and TMPD, the CV curve of $[Fe(CN)_6]^{3-}/[Fe(CN)_6]^{4-}$ shows that the I_{pc} recovered from -0.6429 uA to -7.499 uA along with the △Ep narrowing from 495 mV to 169 mV, showing that a higher degree of changes occurred to the DNA strands on the Au electrode than that of cisplatin only. Figure 2.6c and Figure 2.6d respectively shows the trends of the I_{pc} and the △Ep of $[Fe(CN)_6]^{3-}/[Fe(CN)_6]^{4-}$ over time after the ssDNA-AuE was treated by cisplatin only, and cisplatin in combination with TMPD. In both figures, it is shown that combination of cisplatin and TMPD greatly increased the effect of cisplatin on DNA strand, leading to a stronger recovery of the $[Fe(CN)_6]^{3-}/[Fe(CN)_6]^{4-}$ signal than

that of cisplatin itself.

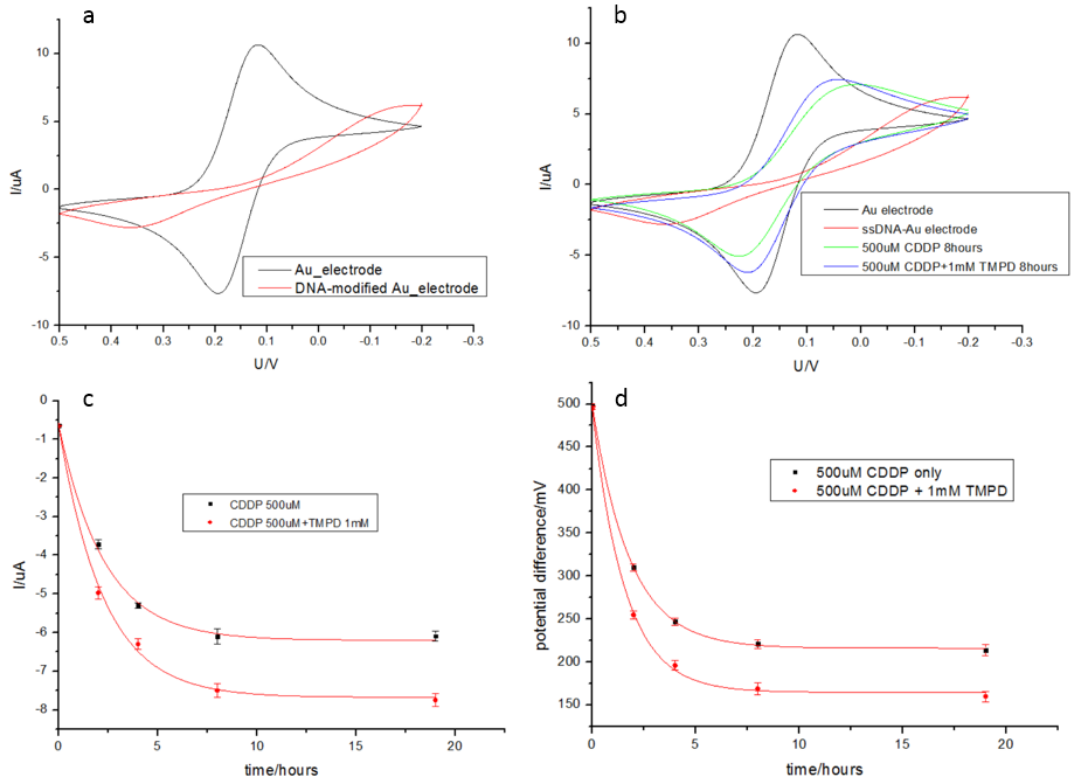

Figure 2.6: (a). CV curves of $[Fe(CN)_6]^{3-}/[Fe(CN)_6]^{4-}$ tested by the bare Au electrode(—) and the ssDNA-AuE (—). (b). CV curves of $[Fe(CN)_6]^{3-}/[Fe(CN)_6]^{4-}$ tested by the ssDNA-AuE after 8 hours treatment by 500 uM CDDP (—), 500 uM CDDP+1 mM TMPD (—). (—) bare Au electrode, (—) ssDNA-AuE. (c). the I_{pc} of $[Fe(CN)_6]^{3-}/[Fe(CN)_6]^{4-}$ tested by the ssDNA-AuE treated by 500 uM CDDP(■), 500 uM CDDP+1 mM TMPD(●) over time. (d). the △Ep of $[Fe(CN)_6]^{3-}/[Fe(CN)_6]^{4-}$ tested by the ssDNA-AuE treated by 500 uM CDDP(■), 500 uM CDDP+1 mM TMPD(●) over time.

Two explanations can account for the $[Fe(CN)_6]^{3-}/[Fe(CN)_6]^{4-}$ signal recovery. First one is the binding of cisplatin on DNA strand. As it mentioned in Chapter 1, cisplatin can bind on DNA bases. Upon the binding of cisplatin on DNA bases, the

chloride anion in cisplatin is replaced by a neutral base molecule, which adds a positive charge to the DNA strand and decreases the negative charge on the DNA strand, and therefore the electrode surface. So the electrical property change due to the binding could recover the $[Fe(CN)_6]^{3-}/[Fe(CN)_6]^{4-}$ electrochemical response. Also, DNA strand break could be the other reason for the recovery of $[Fe(CN)_6]^{3-}/[Fe(CN)_6]^{4-}$ signal. As it demonstrated in Lu's work[9], DNA double strand break was observed in gel electrophoresis experiment. It indicated that DNA strand break can be directly induced by cisplatin instead of being a product of intermediate step during intracellular repair process. Upon the break of DNA strand, the phosphate backbone will leave from the electrode surface, leading to a lower density of negative charges on the electrode surface, so the $[Fe(CN)_6]^{3-}/[Fe(CN)_6]^{4-}$ signal will be recovered.

To explain the interaction between cisplatin and DNA strand, elementary analysis was preformed to gain the information about the DNA modified surfaces. Figure 2.7 shows the XPS spectra of N, P, Au and Pt on the DNA modified Au surface with and without cisplatin treatment. The presence of N and P is observed on the surface (figure 2.7a and b). It is the best evidence of successful DNA modification because these two elements cannot be introduced during sample preparation and treatment. Au signal was acquired to act as a reference. Pt signal was acquired to show the adsorption of cisplatin on DNA strands.

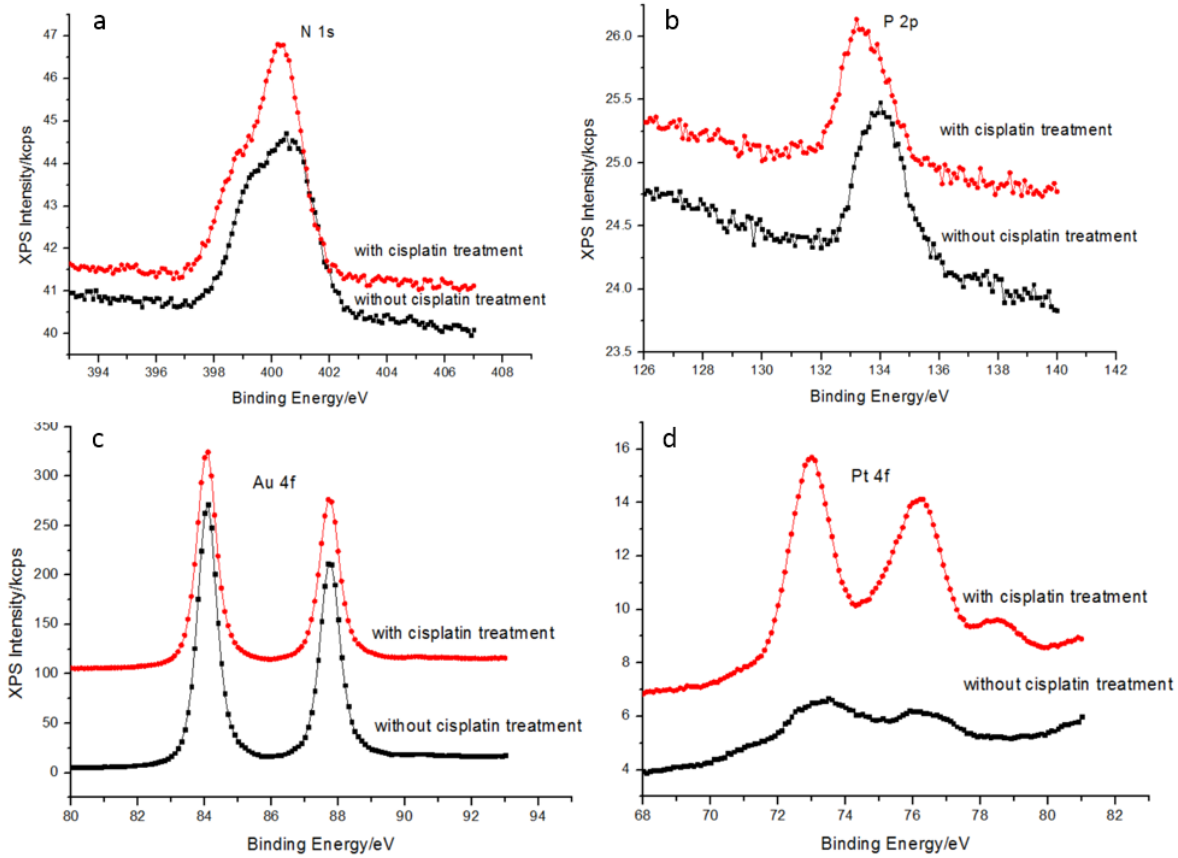

Figure 2.7: High-resolution XPS spectra of the N 1s (a), P 2p (b), Au 4f (c) and Pt 4f (d) regions for the ssDNA modified surface with and without cisplatin treatment

After taking the relative sensitivity factor into account, the percentages of these four elements on the surface were calculated and shown in table 2.1.

element	Without cisplatin treatment	With cisplatin treatment
N	18.91%	23.33%
P	6.77%	5.73%
Au	73.71%	67.00%
Pt	0.62%	3.94%

Table 2.1: percentages of each element on the DNA modified Au surfaces with and without cisplatin treatment.

The decrease of the Au 4f intensity by 6.71 % shows that the surface was covered by more other elements. Meanwhile, it is observed that the signal intensities of N 1s and Pt 4f increased by 4.42 % and 3.32 %, suggesting the binding of cisplatin onto the ssDNA on the Au surface. The P 2p intensity decreased by 1.04 %. Because there is no P element in the structure of cisplatin, the same degree of decrease as Au 4f signal was expected for that of P 2p. So the expected percentage of P element on the surface after cisplatin treatment should be 6.15 %, 0.42 % higher than the actual value. This difference suggested that some P atoms left the surface after the cisplatin treatment. If looking into the N percentage change, the expected N percentage donated from DNA strands should be 17.19 % (the same degree of decrease as Au 4f signal). Assuming two N atoms along with one Pt are attached to the DNA strands for the binding of one cisplatin molecule, the expected N percentage should be 23.83 % (17.19 % + 2*3.32 %), 0.50 % higher than the actual value. As a result, the percentage differences of N and P between the expected and the actual values suggested that a few DNA strands left the surface after cisplatin treatment. In addition, a shift of N and P signal to lower binding energy was observed after the cisplatin treatment. It was reported that a similar shift to higher binding energy was observed for surfaces modified with ssDNA from lower to higher density[79]. So the shift to lower binding energy observed in this project suggested a lower density of DNA covered surface, and therefore suggested the DNA strand break after cisplatin treatment. From the above, it could be concluded that both cisplatin binding and DNA strand break contributed to the recovery of $[Fe(CN)_6]^{3-}$/$[Fe(CN)_6]^{4-}$ signal.

2.3.4 Conclusion

In summary, the Au electrode was successfully modified by using ssDNA through Au-thiol chemistry. By using the redox signal from an indicator, $[Fe(CN)_6]^{3-}/[Fe(CN)_6]^{4-}$, the ssDNA-AuE was successfully characterized. Lower current response of $[Fe(CN)_6]^{3-}/[Fe(CN)_6]^{4-}$ was observed at the ssDNA-AuE compared with bare Au electrode, due to the repulsive force between this redox pair and the DNA strands on the electrode surface. After the ssDNA-AuE was treated by using cisplatin, the recovery of the $[Fe(CN)_6]^{3-}/[Fe(CN)_6]^{4-}$ redox signal indicated the interaction between ssDNA and cisplatin. Elementary analysis suggested that both the binding of cisplatin on DNA strand and DNA strand break contributed to the signal recovery. More interestingly, stronger $[Fe(CN)_6]^{3-}/[Fe(CN)_6]^{4-}$ signal was recovered on the ssDNA-AuE treated by the combination of cisplatin and TMPD than that treated by cisplatin only, showing that this method is sensitive enough to detect the enhanced effect caused by the electron donor TMPD and could be applied to study the effectiveness of the cisplatin based combination chemotherapy.

Chapter 3

Design of the carbon nanomaterials acting as a new generation of electron donor

3.1 Introduction

As it mentioned in Chapter 1, CNMs can act as electron donors due to their electron-rich delocalized π bond. Carrying the basic structure for all CNMs, graphene became the most interesting material since the first day when it was discovered. In Chapter 1, we predicted that graphene is able to donate electrons to cisplatin. Therefore, a strong electron transfer reaction from graphene to cisplatin is expected, thereby boosting the efficacy of this famous anticancer drug. The modified Hummer's method is a common protocol for the synthesis of GO. The GO produced by this method has good solubility in daily used laboratory solvents. However the electronic property of graphene was heavily destructed due to the harsh oxidation environment during the synthesis process. Therefore reduction treatment is needed to recover the electron-rich structure to make the electron transfer reaction from graphene to cisplatin possible.

Graphene and its derivatives have potential applications in many areas such as optical, composite, energy storage and biological materials. In order to use graphene in biological area, the priority is to increase CNMs' solubility and biocompatibility in the physiological environment. As it mentioned in Chapter 1, this problem can be solved by using suitable functionalization, such as grafting hydrophilic polymers.

In this chapter, GO is synthesized through the modified Hummer's method,

followed by the reduction treatment using hydrazine. The Characterization of GO and rGO was done by using atomic force microscopy (AFM), UV-vis spectroscopy and Fourier transform infrared spectroscopy (FT-IR). Afterwards, the rGO was functionalized using amine terminated PEG through carbodiimide chemistry. Finally, the electron donating capability of the PEGylated rGO was tested by the electrochemical methods designed in Chapter 2.

3.2 Materials and method

Chemical and reagents: graphite flakes (100 mesh), potassium persulfate, Hydrazine monohydrate and Poly(ethylene glycol) bis(amine) (M_W=3000) were purchased from Sigma-Aldrich. Phosphorus pentoxide was purchased from EMD. 1-Ethyl-3-(3-dimethylaminopropyl) carbodiimide (EDC) was purchased from GBiosciences. N-Hydroxysuccinimide (NHS) was purchased from Alfa Aesar.

Synthesis of GO: GO was synthesized through the modified Hummer's method as it reported before[30]. Briefly, graphite flakes were pre-oxidized by using $K_2S_2O_8$, P_2O_5 and concentrated H_2SO_4. Afterwards, the pre-oxidized product was subject to extensive oxidation following Hummer's method. The final concentration of the as-synthesized GO was determined after filtration, weighing and re-dissolving, to be 5 mg/ml.

Reduction of GO: the as-synthesized GO was reduced using hydrazine as it reported before[36]. This method can maintain the carboxylic acid groups in GO, while recover the other oxidative defects. To be brief, the GO solution was diluted to a concentration of 2 mg/ml. The diluted solution (7.5 ml) was added to a water solution (7.5 ml) including 1.4 mg/ml hydrazine and 11.2 mg/ml ammonium, followed by 1

hours reaction in a water bath at 95 ℃. The resulted dispersion was dialyzed using Milli-Q water to remove the excess hydrazine in the solution for 5 days with every 4 hours water change. .

UV-vis spectroscopy of GO and rGO: 75 ug/ml GO solution and 25 ug/ml rGO solutions were prepared by using the stock solutions GO and rGO and Milli-Q water. The UV-vis spectra were recorded from 200 nm to 900 nm using a spectrophotometer.

FT-IR and Raman characterization of GO and rGO: 2 ml of 1 mg/ml GO and 2 ml of 1 mg/ml rGO solutions were vacuum filtrated by using PC membranes (25 mm diameter, 0.1 um pore size; Whatman), followed by 5 ml Milli-Q water rinse for three times. The as-prepared GO and rGO membranes were dried overnight in a 70 ℃ oven for FT-IR characterization. Part of the GO and rGO were peeled off from the PC membranes and finely ground with KBr separately (Sigma Aldrich) and compressed into two thin pallets. The FT-IR spectra of GO and rGO were collected by using a Bruker Tensor 37 FTIR spectrometer from 4000 cm-1 to 600 cm-1. The left GO and rGO membranes were characterized using a Horiba Jobin Yvon LabRAM HR 800 Raman spectrometer with a 532 nm excitation laser. The Raman spectra were recorded from 1000 cm^{-1} to 2000 cm^{-1}.

Atomic Force Microscopy (AFM) of GO and rGO: GO and rGO solutions were diluted until their color almost disappear by using HPLC grade ethanol. The diluted solutions were drop casted on fresh cleaved mica surfaces respectively for three minutes, followed by blow-drying using high pure nitrogen gas. The AFM images were collected by using a Nanoscope MultiMode™ AFM instrument (Veeco) in the taping mode. A

silicon probe with a resonant frequency of 300 kHz was used.

PEGylation of rGO: rGO was functionalized by using linear amine terminated PEG through carbodiimide chemistry. Briefly, 10 ml of 1mg/ml rGO solution was added to 5 mL of 2-(N-morpholino)ethanesulfonic acid (MES) buffer solution containing 20 mg amine terminated linear PEG and excess EDC as well as NHS. The mixed solution was kept stirring overnight at room temperature, followed by three days dialysis with every 4 hours water change. The dialyzed solution was centrifuge filtered and re-dissolved until a final concentration of 1.5 mg/ml was achieved and stored for future use.

Solubility test of GO, rGO and PEG-rGO: 200 ul 1 mg/ml GO, rGO and PEG-rGO solutions were mixed with 800 ul PBS (16 mM K2HPO4, 150 mM NaCl, pH 7.2) buffer respectively. All solutions were kept at room temperature for 1 hour and centrifuged at 14000 rpm for 10 mins.

Electrochemical study of PEG-rGO's effect on the interaction between cisplatin and DNA strand: a mixture of 500 uM (0.15 mg/ml) cisplatin and 1.3 mg/ml PEG-rGO were prepared by using the stock cisplatin solution and PEG-rGO solution. The CV curves of 5 mM $[Fe(CN)_6]^{3-}$/$[Fe(CN)_6]^{4-}$ were recorded by using the ssDNA-AuE after the treatment in the prepared solution for 0, 2, 4, 8 and 19 hours.

Effect of PEG-rGO on the interaction between cisplatin and DNA strand: two solutions containing 500 uM (0.15 mg/ml) cisplatin, 500 uM dGMP and different concentration (0.15 mg/ml or 0.75 mg/ml) of PEG-rGO were prepared by using the stock solutions and 0.5 M acetate buffer. Two solutions containing 500 uM (0.15 mg/ml)

cisplatin and different concentration of PEG-rGO (0.15 mg/ml or 0.75 mg/ml) were prepared using the stock solutions and 0.5 M acetate buffer, to collect the background currents. CV curves of the two solutions containing dGMP were recorded after 0, 5, 10, 24 and 48 hours incubation, using the same GCE and the potentiostat in Chapter 2. The background CV current was recorded by using the two solutions without dGMP after 0, 5, 10, 24 and 48 hours incubation.

Clonogenic assay of HeLa cells: Reasonable number of HeLa cells were seeded in 5 six-well plates (Thermo scientific) respectively and treated by 0.1, 0.5, 1, 2 and 5 uM cisplatin and 0.1, 0.5, 1, 2 and 5 uM cisplatin plus 10ug/ml PEG-rGO for 2 hours (each treatment containing three parallel experiments). Following this, the treated cells were incubated for 7 days and dyed by crystal purple. The cell viability in each group was determined based on the colonies formed after the incubation.

3.3 Results and Discussion

GO and rGO were successfully synthesized as shown in Figure 3.1a and b. the color of rGO is more black than that of GO, owing to the removal of the defects from the GO structure after reduction. This change can be theoretically shown by the UV-vis absorption spectra of GO and rGO (Figure 3.1c). Compared with GO, the absorption peak of rGO shifted from 227 nm to 262 nm, indicating the restored aromatic C=C bond after reduction[36]. At the same time, the shoulder peak around 300 nm in the spectrum of GO, which can be attributed to the transitions of C=O bond[93], disappeared in that of rGO, demonstrating a decreased oxygen level in rGO structure. Both these changes showed that the GO was effectively reduced and the electronic property of graphene

was recovered.

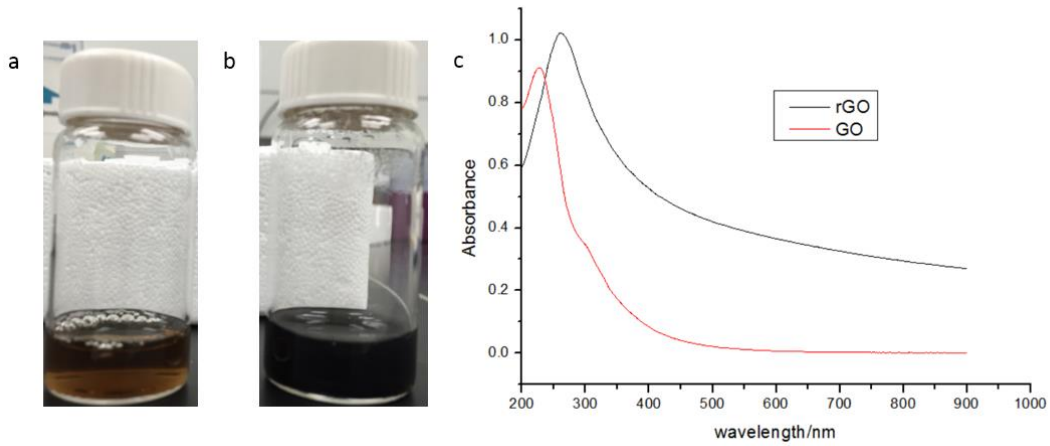

Figure 3.1: as-synthesized (a) GO solution and (b) rGO solution (c) UV-vis absorption spectra of GO and rGO.

Figure 3.2a and b are the AFM images of as-synthesized GO and rGO sheets on fresh cleaved mica substrates. The lateral size of the as-synthesized GO ranges from hundreds of nanometers to several micrometers. The thickness of the GO is ~1.1 nm, while rGO is ~0.7 nm as shown in Figure 3.2c and d. Compared with GO, the thickness of rGO is ~0.4 nm thinner. However, it was reported that the oxygen-containing functionalized groups are sized in around 100 picometers range[94]. So the removal of these oxygen-containing groups cannot straightforwardly explain the observed decrease in the height profile. However, it is well-known that for all AFM experiments conducted in air environment, a thin layer of water always exists on the sample. So the removal of the hydrophilic oxygen-containing groups can potentially decrease the amount of the thin layer of water on rGO, therefore making the tested rGO thickness much thinner than that of GO.

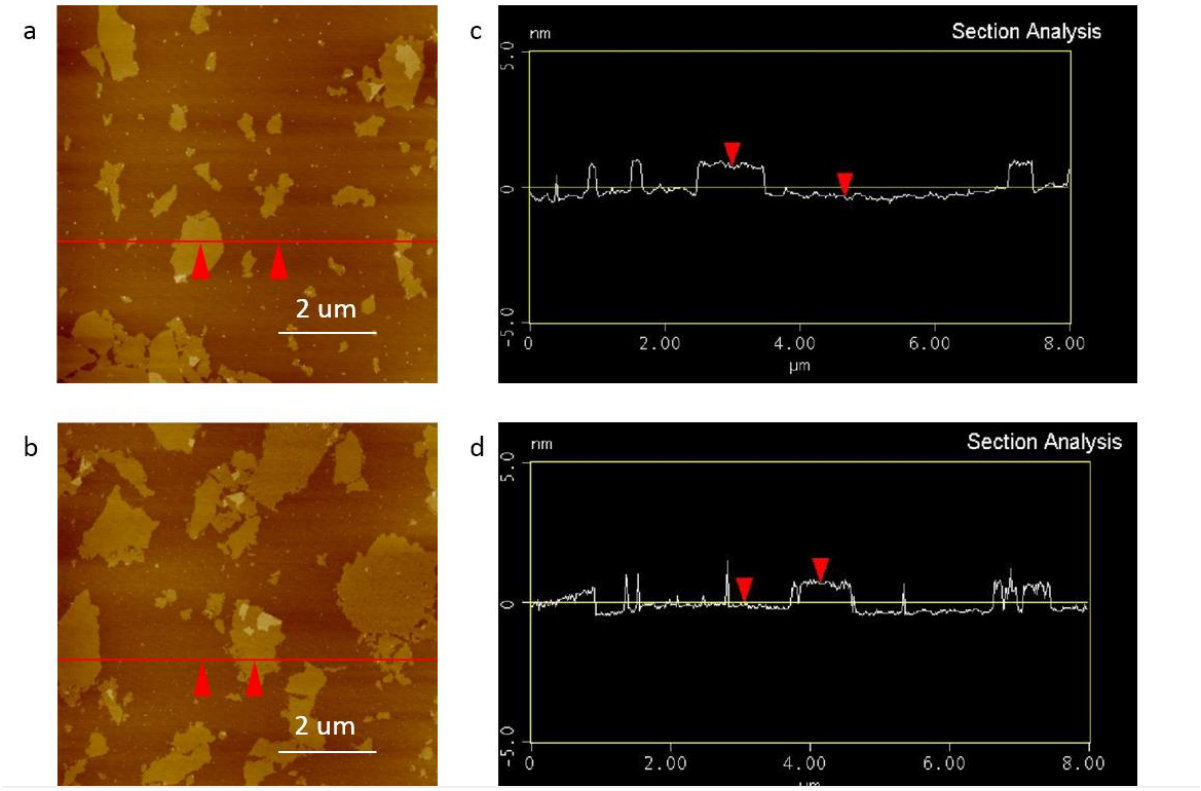

Figure 3.2: AFM images of (a) GO and (b) rGO. (c) Height profile along the line drawn in (a), showing the thickness of GO (~1.1 nm). (d) Height profile long the line drawn in (b), showing the thickness of rGO (~0.7 nm).

The Raman spectra of GO and rGO are shown in Figure 3.3. The characterization peaks of GO and rGO are respectively the D band at ~1350 cm^{-1} and the G band at ~ 1590 cm^{-1}. It is reported that the D band arises from defect mediated zone-edge (near K-point) phonons, whereas the G band is attributed to the doubly degenerate E2g mode at the Brillouin zone center[30]. The intensity of the D band /G band ratio (I_D/I_G) is widely used for determining the degree of defect in graphene-related materials. From the Raman spectra of GO and rGO, it is shown that the I_D/I_G increased from 0.86 for GO to 1.07 for rGO, indicating a decrease in the average size of the sp2 domains upon the reduction of GO. This change is typical for hydrazine reduced GO and can be explained, for the reduced GO, new graphene-like domains created after the reduction

are smaller in size than the ones present in the GO films before the reduction, but more numerous in number. As a result, the electronic property of graphene is still restored, even though the I_D/I_G increases in Raman spectra.

Stabilities of GO, rGO and PEG-rGO in physiological environment were studied by using the saline solution. After mixed with PBS buffer and treated by the high-speed centrifugation, the status of all the three samples are shown in Figure 3.4. Both GO and rGO have very poor stabilities after mixed with PBS buffer, while PEG-rGO is much more stable after all the treatment. This result showed the effectiveness the PEGylation, and meanwhile suggested the success of the PEG functionalization.

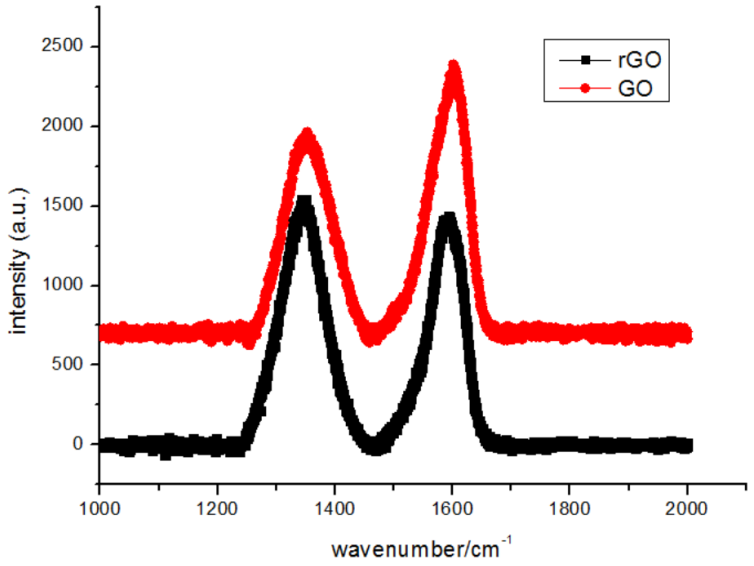

Figure 3.3: Raman spectra of GO and rGO.

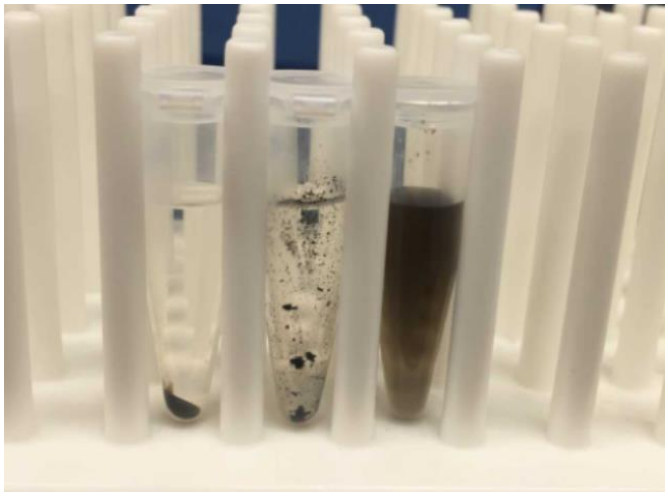

Figure 3.4: The solutions of GO, rGO and PEG-rGO (from left to right) after 1 hour of PBS buffer treatment and 10 mins of centrifugation.

After the fabrication of the stable PEG-rGO, the electrochemical study of PEG-rGO's effect on the interaction between cisplatin and DNA strand was conducted by using the methods developed in Chapter 2. The recovery of the $[Fe(CN)_6]^{3-}/[Fe(CN)_6]^{4-}$ signal was recorded after the ssDNA-AuE was treated in a solution containing 500 uM cisplatin and 1.3 mg/ml PEG-rGO for 8 hours (Figure 3.5a). Compared with 500 uM cisplatin only, the combination of 500 uM cisplatin and 1.3 mg/ml PEG-rGO did not show much noticeable difference in the change of either the I_{pc} or the $\triangle$Ep value. Figure 3.5b shows that the I_{pc} of $[Fe(CN)_6]^{3-}/[Fe(CN)_6]^{4-}$ tested by ssDNA-AuE treated with 500 uM cisplatin only and cisplatin in combination with 1.3 mg/ml PEG-rGO over time. The nearly identical I_{pc} at various time points showed that the PEG-rGO basically had no effect on the interaction between cisplatin and DNA strand.

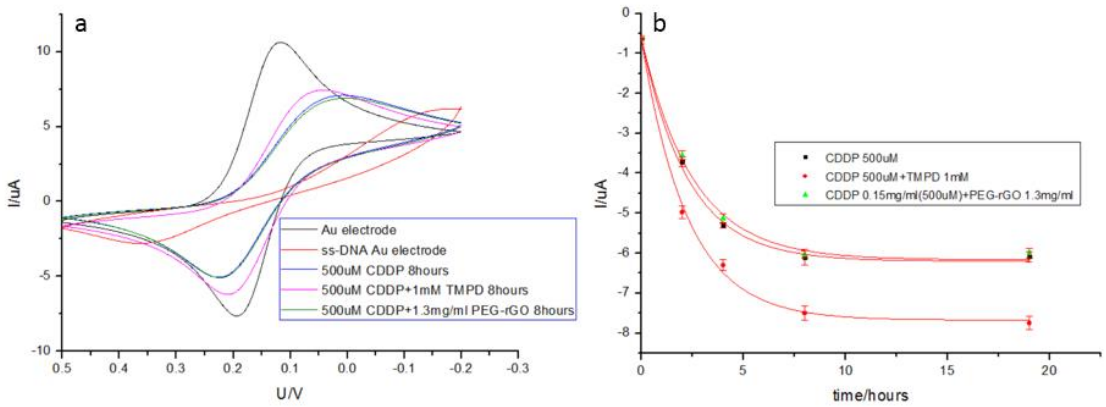

Figure 3.5: (a). CV curves of $[Fe(CN)_6]^{3-}/[Fe(CN)_6]^{4-}$ tested by the bare Au electrode(—), the ssDNA-AuE (—), CV curves of $[Fe(CN)_6]^{3-}/[Fe(CN)_6]^{4-}$ tested by ssDNA-AuE after 8 hours treatment by 500 uM CDDP (—), 500 uM CDDP+1 mM TMPD (—) and 500 uM CDDP + 1.3 mg/ml PEG-rGO. (b). the I_{pc} of $[Fe(CN)_6]^{3-}/[Fe(CN)_6]^{4-}$ at various time points after ssDNA-AuE treated by 500 uM CDDP(■), 500 uM CDDP+1 mM TMPD(●) and 500 uM CDDP+1.3 mg/ml PEG-rGO(▲).

In addition, the electrochemical method using the oxidation signal of G base as an indicator was also applied to study the effect of PEG-rGO on the interaction between DNA and cisplatin. In this experiment, the dGMP oxidation peak exhibited nearly identical trends over time, no matter in the presence of PEG-rGO or not (Figure A.1), supporting the results from the ssDNA-AuE electrochemistry.

Figure 3.6 shows the survival percentage of HeLa cells after treated by cisplatin only and cisplatin in combination with PEG-rGO in the clonogenic assay. Compared with the groups treated by cisplatin only, the groups treated by cisplatin in combination with PEG-rGO didn't show any noticeable enhanced cell killing, which is consistent

with the results got from the electrochemical study. So above all, it could be concluded that PEG-rGO, not as expected, cannot enhance the efficacy of cisplatin.

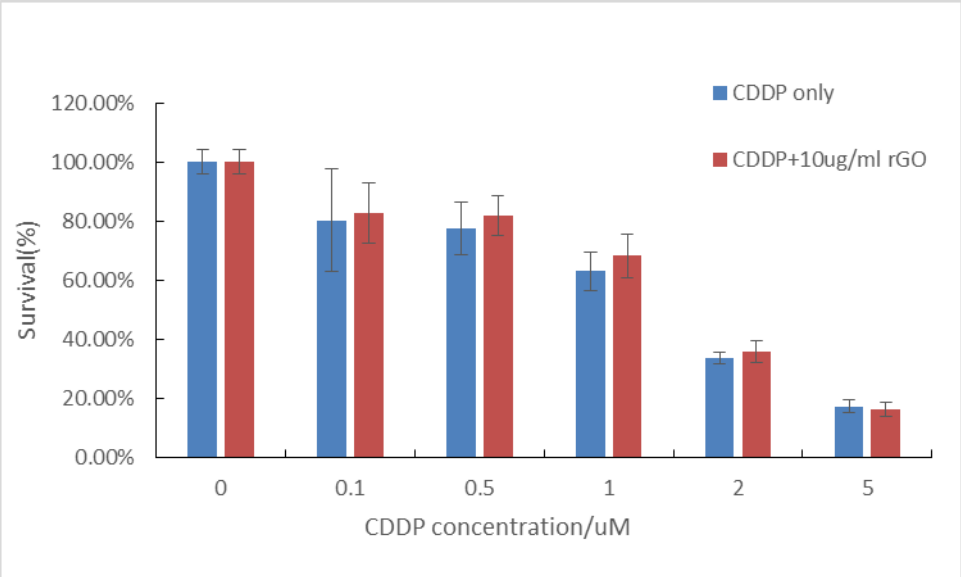

Figure 3.6: Clonogenic assay of HeLa cells with treatment of cisplatin alone and in combination with PEG-rGO.

It is reported that Pt nanoparticles (Pt NPs) can be produced from H_2PtCl_6 and GO by heat or reducing agents, such as $NaBH_4$[95,96]. So after the electron transfer reaction between cisplatin and rGO, it is possible that some cisplatin radicals can be adsorbed on the PEG-rGO nanosheets, preventing the leaving of these radicals, and therefore the attacking to DNA strands. In addition, the absence of electron transfer reaction between cisplatin and PEG-rGO could be another reason for the lack of enhanced effect, so very similar results were observed no matter in the presence of PEG-rGO or not. Therefore, future work is needed to confirm why PEG-rGO is not able to enhance the efficiency of cisplatin, so that a better design can be made.

3.4 Conclusion

In conclusion, rGO was successfully fabricated through the modified Hummer's method followed by hydrazine reduction. The UV-vis spectra and AFM images showed that, after the reduction, most of the oxygen containing groups were removed from the GO surface, and the electronic property of graphene was recovered. Furthermore, rGO was successfully functionalized by linear PEG using carbodiimide chemistry and the PEGylation was verified by the solubility test. The effect of PEG-rGO on the interaction between cisplatin and DNA was investigated, using the electrochemical methods described in Chapter 2 along with the Clonogenic assay. None of these experiments showed noticeable enhanced cisplatin efficiency when combining cisplatin and PEG-rGO. The formation of Pt NPs or the absence of electron transfer reaction between cisplatin and PEG-rGO could be the reason for the lack of enhanced cisplatin efficiency. Therefore, future work is needed to make graphene an effective electron donor.

Chapter 4

Summary

Cisplatin is an anticancer chemotherapy drug used for treating a wide range of cancers. The hydrolysis mechanism is long believed the initial action of this drug. So based this mechanism, over 3000 of cisplatin analogues were synthesized to reduce the side effect and increase the treatment efficacy. However only oxaliplatin and carboplatin were approved by FDA, suggesting that the hydrolysis mechanism might not be the right principle behind cisplatin toxicity. Recently, by using a femtosecond time-resolved laser spectroscopy, an electron transfer reaction mechanism of cisplatin and DNA was proposed. Based on this mechanism, it is observed that the combination of cisplatin and an electron donor can dramatically increase the efficacy of cisplatin, opening a new gate for the design of cisplatin based combination chemotherapy.

As the most popular material in the past decade, graphene attracted tons of attention because of its unique electronic and mechanical properties. The delocalized π bond structure makes graphene a potential electron donor, making it possible to establish a new generation of combination therapy by using cisplatin and CNMs.

The electrochemical method is a powerful tool to get DNA related information such as DNA base damage, DNA strand break, DNA sequencing and DNA hybridization. In Chapter 2, two electrochemical methods were designed, using the redox signal of DNA bases, and an indicator species along with the ssDNA-AuE, to study the DNA damage. In the first method, the interaction between cisplatin and dGMP

was characterized and studied by the decrease in the dGMP oxidation peak. However, by using this method, the combination of cisplatin and TMPD didn't lead to faster or more pronounced decrease in the dGMP oxidation peak compared with cisplatin itself, probably due to the autoionization of TMPD in water. In the second method, ssDNA-AuE was fabricated and the interaction between cisplatin and ssDNA was monitored by the redox signal change of a pair of indicator, $[Fe(CN)_6]^{3-}/[Fe(CN)_6]^{4-}$. Briefly, compared with the bare Au electrode, decrease of the $[Fe(CN)_6]^{3-}/[Fe(CN)_6]^{4-}$ redox signal was observed at the ssDNA-AuE, due to the repulsive force between the ssDNA and the negatively charged indicator. After the ssDNA-AuE was treated by cisplatin, the redox signal of $[Fe(CN)_6]^{3-}/[Fe(CN)_6]^{4-}$ recovered, suggesting that cisplatin reduced the repulsive force between this indicator and the ssDNA. Elementary analysis confirmed that both cisplatin binding and DNA strand break contributed to the recovery of $[Fe(CN)_6]^{3-}/[Fe(CN)_6]^{4-}$ signal. More interestingly, stronger $[Fe(CN)_6]^{3-}/[Fe(CN)_6]^{4-}$ signal was recovered on the ssDNA-AuE treated by the combination of cisplatin and TMPD than that on the same electrode treated by cisplatin only, showing that this method is sensitive enough to detect the enhanced effect caused by TMPD and could be applied to study the effectiveness of the cisplatin based combination chemotherapy.

In chapter 3, rGO was synthesized through the modified Hummer's method followed by hydrazine reduction. UV-vis and AFM characterization showed that the oxygen containing groups were successfully removed from GO nanosheets, and the electronic property of graphene was recovered. Furthermore, rGO was successfully functionalized by linear PEG using carbodiimide chemistry and the PEGylation was

verified by the solubility test. After the fabrication, the effect of PEG-rGO on the interaction between cisplatin and DNA was investigated, by using the methods designed in Chapter 2 as well as the in vitro experiment. However, all experiment results point to the conclusion that PEG-rGO has no noticeable impact on improving cisplatin efficacy. The formation of Pt NPs or the absence of electron transfer reaction between cisplatin and PEG-rGO could be the reason why no enhanced cisplatin efficacy can be observed. Therefore, future work is needed to make graphene an effective electron donor.

Our study, for the first time, used the intrinsic DNA signal and the signal from indicator species along with the ssDNA-AuE to detect DNA damage caused by cisplatin. DNA base damage and DNA strand damage were respectively detected by these two methods. In addition, our work for the first time designed a CNM and cisplatin based combination chemotherapy, which can be a reference for similar future research.

Chapter 5

Future work

Even though two electrochemical methods were designed to detect DNA damage, some changes could be done to improve them. For PEG-rGO, because no enhanced DNA damage or cell killing was observed when combining with cisplatin, the design of an effective graphene based material which can act as an electron donor still need to continue.

First, in the electrochemical method using the dGMP oxidation signal as an indicator, the combination of cisplatin and TMPD didn't lead to faster or more pronounced decrease in the dGMP oxidation peak compared with cisplatin itself. The instability of TMPD in aqueous solution makes it hard to tell whether it is the method itself or the autoionization of TMPD causing the failure to observe the enhanced dGMP decrease. To verify the effectiveness of this method, it is important to rule out the interference from TMPD autoionization. So instead of water, some other non-aqueous solvents can be used to prepare the experiment solutions to avoid the occurrence of TMPD autoionization. The eligible solvent should meet the requirements including, the ability to dissolve cisplatin, TMPD, DNA bases (or their derivatives) and suitable electrolyte, and a low binding energy of solvated electron, so that TMPD can be stabilized in the solvent. Alternatively, replacing TMPD by some other electron donors which are stable in aqueous solutions is also a good choice to rule out the interference from TMPD autoionization.

Second, it is well-known that DNA double strand break is important to induce cell death. So if our DNA modified electrode can be used for detecting DNA double strand break, it could be more useful for testing the efficacy of cisplatin or some other anticancer drugs compared with the current design. To realize this detection, we can hybridize the ssDNA on the Au electrode by its complementary DNA, so that a double-stranded DNA modified surface can be generated. By recording the similar electrochemical signal change described in this project and XPS data, the information about DNA double strand break could be collected. Furthermore, DNA strands with unique sequence, for example G base-rich DNA strand, can be used to improve the sensitivity of the detection.

Finally, the reason why PEG-rGO cannot enhance cisplatin efficacy should be uncovered so that an effective graphene based electron donor can be designed. To confirm the formation of Pt NPs, elementary analysis can be used. Briefly, a graphene covered surface can be prepared by drop casting, or some other method such as chemical vapor deposition, followed by soaking in a cisplatin solution for certain time. If the Pt signal can be detected on the surface, the formation of Pt NPs will be confirmed. If no Pt signal can be detected on the surface, it might imply that there is no electron transfer reaction between cisplatin and PEG-rGO. In the case of the second situation, some functionalization will be needed to make graphene an effective electron donor. For example, some electron donating molecules can be linked on the structure of graphene nanosheets, such as porphyrin or oligothiophene[97,98]. It is expected that electrons can transfer from the electron donating molecule either directly to cisplatin or

to graphene at first, then cisplatin. In addition, we can also dope graphene using some active metal atoms, to slightly change its electronic property, therefore making it a more effective electron donor compared with the bare graphene.

Appendix

FT-IR and Raman characterization of GO and rGO:

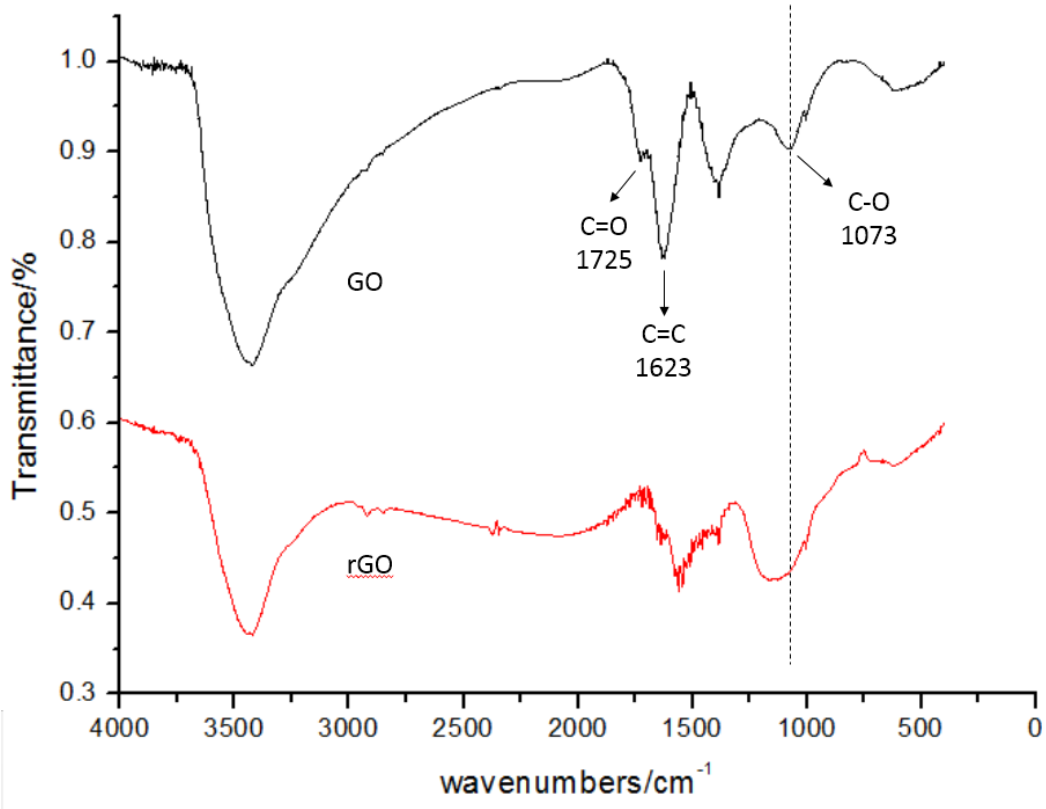

Figure A.1: FT-IR spectra of GO and rGO.

For the FT-IR spectra, the C=C absorption in rGO shifted to a lower wavenumber than that in GO. In addition, the C-O absorption in the spectrum of GO disappeared in that of rGO, indicating the leaving of hydroxyl and epoxy groups from the surface of GO.

Effect of PEG-rGO on the interaction between cisplatin and DNA base:

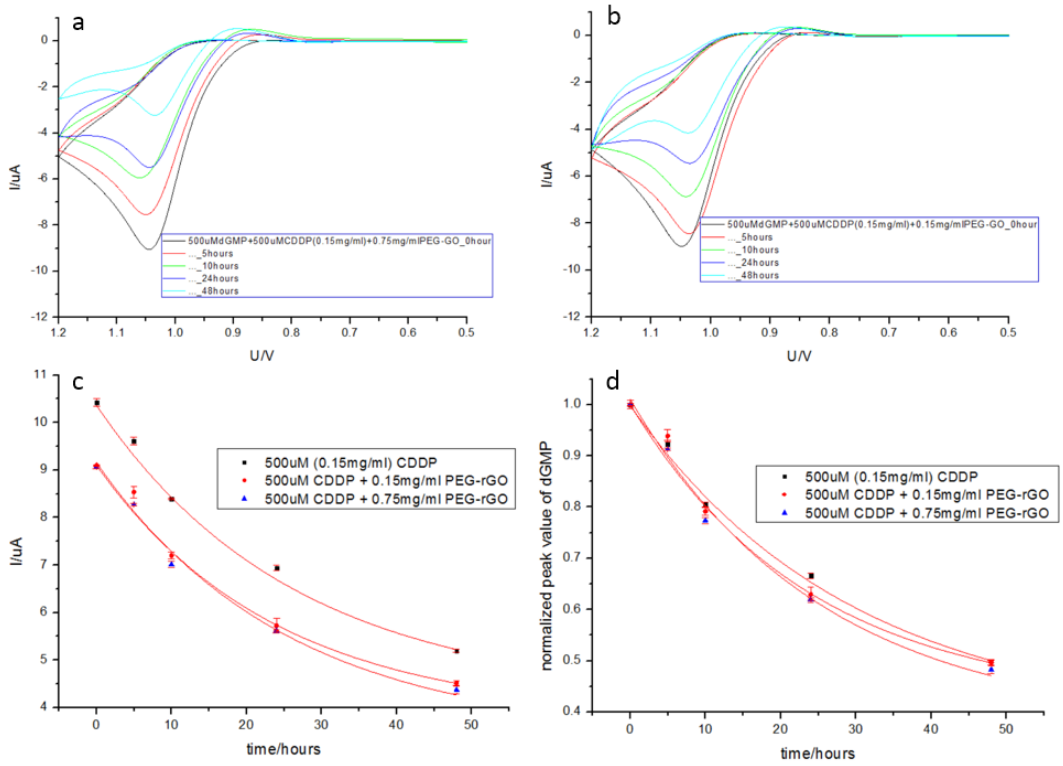

Figure A.2: Background subtracted CV curves of 500 uM dGMP mixed with 500 uM CDDP and (a) 0.15 mg/ml, (b) 0.75 mg/ml PEG-rGO at various time points. Scan rate: 20 mV/s. (c) Oxidation peak value of 500 uM dGMP mixed with 500 uM CDDP (■), 500 uM CDDP+ 0.15 mg/ml PEG-rGO (●) and 500 uM CDDP+ 0.75 mg/ml PEG-rGO (▲) over time. (d) Normalized oxidation peak value of 500 uM CDDP (■), 500 uM CDDP+ 0.15 mg/ml PEG-rGO (●) and 500 uM CDDP+ 0.75 mg/ml PEG-rGO (▲) over time.

References

1. Wang, D. & Lippard, S. J. Cellular processing of platinum anticancer drugs. *Nat. Rev. Drug Discov.* **4,** 307–320 (2005).
2. Reedijk, J. New clues for platinum antitumor chemistry: kinetically controlled metal binding to DNA. *Proc. Natl. Acad. Sci. U. S. A.* **100,** 3611–3616 (2003).
3. Rosenberg, B., VanCamp, L., Trosko, J. E. & Mansour, V. H. Platinum compounds: a new class of potent antitumour agents. *Nature* **222,** 385–386 (1969).
4. Stewart, J. M. *et al.* Phenotypic heterogeneity and instability of human ovarian tumor-initiating cells. *Pnas* **108,** 6468–6473 (2011).
5. Galluzzi, L. *et al.* Molecular mechanisms of cisplatin resistance. *Oncogene* **31,** 1869–1883 (2012).
6. Raymond, E., Faivre, S., Chaney, S., Woynarowski, J. & Cvitkovic, E. Cellular and molecular pharmacology of oxaliplatin. *Mol. Cancer Ther.* **1,** 227–235 (2002).
7. Hambley, T. W. The influence of structure on the activity and toxicity of Pt anti-cancer drugs. *Coord. Chem. Rev.* **166,** 181–223 (1997).
8. Lu, Q. B. Molecular reaction mechanisms of combination treatments of low-dose cisplatin with radiotherapy and photodynamic therapy. *J. Med. Chem.* **50,** 2601–2604 (2007).
9. Luo, T. *et al.* Electron transfer-based combination therapy of cisplatin with tetramethyl-p-phenylenediamine for ovarian, cervical, and lung cancers. *Proc.*

Natl. Acad. Sci. **109,** 10175–10180 (2012).

10. Lu, Q-B. *et al*. Electron Transfer Reaction Mechanism of Cisplatin with DNA at the Molecular Level. *Molecular pharmaceutics* **4,** 624–628 (2007).
11. Ando, T. The electronic properties of graphene and carbon nanotubes. *NPG asia materials* **1,** 17–21 (2009).
12. Castro Neto, A. H. The electronic properties of graphene. *Reviews of modern physics* **81,** 109–162 (2009).
13. Liu, Z., Robinson, J. T., Tabakman, S. M., Yang, K. & Dai, H. Carbon materials for drug delivery & cancer therapy. *Mater. Today* **14,** 316–323 (2011).
14. Palecek, E. Past, present and future of nucleic acids electrochemistry. *Talanta* **56,** 809–819 (2002).
15. Palecek E, Bartosik M. Electrochemistry of Nucleic Acids. *Chemical Reviews* 112(6): 3427-3481. (2012).
16. Wang, D. & Lippard, S. J. Cellular processing of platinum anticancer drugs. *Nat. Rev. Drug Discov.* **4,** 307–20 (2005).
17. Hong, G., Diao, S., Antaris, A. L. & Dai, H. Carbon Nanomaterials for Biological Imaging and Nanomedicinal Therapy. *Chem. Rev.* (2015).
18. Pinto, H. & Markevich, A. Electronic and electrochemical doping of graphene by surface adsorbates. *Beilstein J. Nanotechnol.* **5,** 1842–1848 (2014).
19. Chen, Z. *et al*. Surface transfer hole doping of epitaxial graphene using MoO3 thin film. *Appl. Phys. Lett.* **96,** (2010).
20. Liu, H., Liu, Y. & Zhu, D. Chemical doping of graphene. *J. Mater. Chem.* **21,**

3335 (2011).

21. Chen, W., Chen, S., Dong, C. Q., Xing, Y. G. & Wee, A. T. S. Surface transfer p-type doping of epitaxial graphene. *J. Am. Chem. Soc*. **129,** 10418–10422 (2007).

22. Crowther, A. C., Ghassaei, A., Jung, N. & Brus, L. E. Strong charge-transfer doping of 1 to 10 layer graphene by NO_2. *ACS Nano* **6,** 1865–1875 (2012).

23. Rao, C. N. R. & Voggu, R. Charge-transfer with graphene and nanotubes. *Mater. Today* **13,** 34–40 (2010).

24. Voggu, R., Das, B., Rout, C. S. & Rao, C. N. R. Effects of charge transfer interaction of graphene with electron donor and acceptor molecules examined using Raman spectroscopy and cognate techniques. *J. Phys. Condens. Matter* **20,** 472204 (2008).

25. Das, B., Voggu, R., Rout, C. S. & Rao, C. N. R. Changes in the electronic structure and properties of graphene induced by molecular charge-transfer. *Chem. Commun. (Camb).* 5155–5157 (2008).

26. Choudhury, D., Das, B., Sarma, D. D. & Rao, C. N. R. XPS evidence for molecular charge-transfer doping of graphene. *Chem. Phys. Lett.* **497,** 66–69 (2010).

27. Giovannetti, G. *et al.* Doping graphene with metal contacts. *Phys. Rev. Lett.* **101,** 3–6 (2008).

28. William S. Hummers, J. & Offeman, R. E. Preparation of Graphitic Oxide. *J. Am. Chem. Soc* **80,** 1339 (1958).

29. Marcano, D. C. *et al.* Improved synthesis of graphene oxide. *ACS Nano* **4,** 4806–

4814 (2010).

30. Gao, X. & Tang, X. (Shirley). Effective reduction of graphene oxide thin films by a fluorinating agent: Diethylaminosulfur trifluoride. *Carbon N. Y.* **76,** 133–140 (2014).

31. Zhang, Y., Zhang, L. & Zhou, C. Review of chemical vapor deposition of graphene and related applications. *Acc. Chem. Res.* **46,** 2329–2339 (2013).

32. Pei, S. & Cheng, H. M. The reduction of graphene oxide. *Carbon N. Y.* **50,** 3210–3228 (2012).

33. Stankovich, S. *et al.* Stable aqueous dispersions of graphitic nanoplatelets via the reduction of exfoliated graphite oxide in the presence of poly(sodium 4-styrenesulfonate). *J. Mater. Chem.* **16,** 155 (2006).

34. Stankovich, S. *et al.* Synthesis of graphene-based nanosheets via chemical reduction of exfoliated graphite oxide. *Carbon N. Y.* **45,** 1558–1565 (2007).

35. McAllister, M. J. *et al.* Single sheet functionalized graphene by oxidation and thermal expansion of graphite. *Chem. Mater.* **19,** 4396–4404 (2007).

36. Li, D., Müller, M. B., Gilje, S., Kaner, R. B. & Wallace, G. G. Processable aqueous dispersions of graphene nanosheets. *Nat. Nanotechnol.* **3,** 101–105 (2008).

37. Sun, X. *et al.* Nano-Graphene Oxide for Cellular Imaging and Drug Delivery. *Nano Res.* **1,** 203–212 (2008).

38. Liu, Z., Robinson, J. T., Sun, X. & Dai, H. PEGylated Nanographene Oxide for Delivery of Water-Insoluble Cancer Drugs. *Journal of the American Chemical*

Society. **130(33),**10876–10877 (2008).

39. Banerjee, S. S., Aher, N., Patil, R. & Khandare, J. Poly(ethylene glycol)-Prodrug Conjugates: Concept, Design, and Applications. *J. Drug Deliv.* **2012,** 1–17 (2012).

40. Ma, X. *et al.* A functionalized graphene oxide-iron oxide nanocomposite for magnetically targeted drug delivery, photothermal therapy, and magnetic resonance imaging. *Nano Res.* **5,** 199–212 (2012).

41. Yang, K., Feng, L., Hong, H., Cai, W. & Liu, Z. Preparation and functionalization of graphene nanocomposites for biomedical applications. *Nat. Protoc.* **8,** 2392–403 (2013).

42. Coleman, M. & Tang, X. Diffusive transport of two charge equivalent and structurally similar ruthenium complex ions through graphene oxide membranes. *Nano Res.* **8,** 1128–1138 (2015).

43. Meyers, J. A., Sanchez, D., Elwell, L. P. & Falkow, S. Simple Agarose Gel Electrophoretic Method for the Identification and Characterization of Plasmid Deoxyribonucleic Acid. *J. Bacteriol.* **129,** 1171 (1977).

44. Nguyen, J. *et al.* Direct observation of ultrafast-electron-transfer reactions unravels high effectiveness of reductive DNA damage. *Proc. Natl. Acad. Sci. U. S. A.* **108,** 11778–11783 (2011).

45. Kassie, F., Parzefall, W. & Knasmüller, S. Single cell gel electrophoresis assay: a new technique for human biomonitoring studies. *Mutat. Res.* **463,** 13–31 (2000).

46. Herschleb, J., Ananiev, G. & Schwartz, D. C. Pulsed-field gel electrophoresis. *Nat. Protoc.* **2,** 677–684 (2007).

47. Strathdee, F. & Free, A. Denaturing gradient gel electrophoresis (DGGE). *Methods Mol. Biol.* **1054,** 145–57 (2013).

48. Macgregor, J. T. & Johnson, I. J. In vitro metabolic activation of ethidium bromide and other phenanthridinium compounds: mutagenic activity in Salmonella typhimurium. *Mutat. Res.* **48,** 103–107 (1977).

49. Jenner, a, England, T. G., Aruoma, O. I. & Halliwell, B. Measurement of oxidative DNA damage by gas chromatography-mass spectrometry: ethanethiol prevents artifactual generation of oxidized DNA bases. *Biochem. J.* **331 (Pt 2,** 365–369 (1998).

50. Dawidzik, J. B. *et al.* DNA damage measured by liquid chromatography-mass spectrometry in mouse fibroblast cells exposed to oxidative stress. *Biochim. Biophys. Acta - Gen. Subj.* **1621,** 211–217 (2003).

51. Gabelica, V. Nucleic Acids in the Gas Phase. *Springer*. 203–224 (2014).

52. Dizdaroglu, M. Chemical determination of free radical-induced damage to DNA. *Free Radic. Biol. Med.* **10,** 225–242 (1991).

53. Dizdaroglu, M., Jaruga, P., Birincioglu, M. & Rodriguez, H. Free radical-induced damage to DNA: Mechanisms and measurement. *Free Radic. Biol. Med.* **32,** 1102–1115 (2002).

54. Dizdaroglu, M. Quantitative determination of oxidative base damage in DNA by stable isotope-dilution mass spectrometry. *FEBS Lett.* **315,** 1–6 (1993).

55. Hwang, E.-S. & Bowen, P. E. DNA damage, a biomarker of carcinogenesis: its measurement and modulation by diet and environment. *Crit. Rev. Food Sci. Nutr.* **47,** 27–50 (2007).

56. Shmuel, A. Identification of Programmed Cell Death In Situ. *Cell* **119,** 493–501 (1992).

57. Negoescu, A. *et al.* TUNEL : Improvement and Evaluation of the Method for In Situ Apoptotic Cell Identification. *Biochemica* 12–17 (1997).

58. Prokhorova, G. V, Osipova, E. A. & Gurentsova, O. I. Polarographic Behaviour of Molybdogermanic Heteropoly Acid. *Vestn. Mosk. Univ. Seriya Khimiya* **32,** 496–500 (1991).

59. Smith, D. L., & Elving, P. J. Electrochemical reduction of purine, adenine and related compounds: polarography and macroscale electrolysis. *Journal of the American Chemical Society*, ***84*****(8)**, 1412-1420. (1960).

60. Arbor, a N. N. & Smith, L. Electrochemical Reduction of Pyrimidine, Cytosine and Related Compounds. *Polarography and Macroscale Electrolysis*. **18,** 123-126, (1962).

61. Janík, B., & Paleček, E. Polarographic behavior of cytosine and some of its derivatives. *Archives of biochemistry and biophysics*, ***105*****(2)**, 225-236, (1964)

62. Cummings, T. E., Jensen, M. a. & Elving, P. J. Adenine and Cytosine: Basic Polarographic Behavior and Its Interpretation. *Bioelectrochemistry Bioenerg.* **5,** 239 (1978).

63. Palecek, E., Jelen, F. & Trnková, L. Cyclic voltammetry of DNA at a mercury

electrode: an anodic peak specific for guanine. *Gen. Physiol. Biophys.* **5,** 315–329 (1986).

64. Dryhurst, G. Electrochemical Oxidation of 6-Thiopurine at the Pyrolytic Graphite Electrode. *J. Electrochem. Soc.* **116,** 1097 (1969).

65. Dryhurst, G. & Elving, P. J. Electrochemical Oxidation of Adenine: Reaction Products and Mechanisms. *J. Electrochem. Soc.* **115,** 1014 (1968).

66. Oliveira-Brett, a. M., Piedade, J. a P., Silva, L. a. & Diculescu, V. C. Voltammetric determination of all DNA nucleotides. *Anal. Biochem.* **332,** 321–329 (2004).

67. Stempkowska, I., Ligaj, M., Jasnowska, J., Langer, J. & Filipiak, M. Electrochemical response of oligonucleotides on carbon paste electrode. *Bioelectrochemistry* **70,** 488–494 (2007).

68. Wang, X. X., Gu, Y., Fang, Y. F. & Huang, Y. P. Mechanism of oxidative damage to DNA by Fe-loaded MCM-41 irradiated with visible light. *Chinese Sci. Bull.* **57,** 1504–1509 (2012).

69. Gedik, C. M., Wood, S. G. & Collins, a R. Measuring oxidative damage to DNA; HPLC and the comet assay compared. *Free Radic. Res.* **29,** 609–615 (1998).

70. Oliveira-Brett, a. M., Vivan, M., Fernandes, I. R. & Piedade, J. a P. Electrochemical detection of in situ adriamycin oxidative damage to DNA. *Talanta* **56,** 959–970 (2002).

71. Oliveira-Brett, A. M. & Diculescu, V. C. Electrochemical study of quercetin-DNA interactions: Part II. In situ sensing with DNA biosensors.

Bioelectrochemistry **64,** 143–150 (2004).

72. Wang, J. *et al.* DNA Biosensor for the Detection of Hydrazines. *Society* **68,** 2251–2254 (1996).

73. Brabec, V. DNA sensor for the determination of antitumor platinum compounds. *Electrochimica Acta* **45,** 2929–2932 (2000).

74. Millan, K. M. & Mikkelsen, S. R. Sequence-selective biosensor for DNA based on electroactive hybridization indicators. *Anal. Chem.* **65,** 2317–2323 (1993).

75. Hashimoto, K., Ito, K. & Ishimori, Y. Sequence-specific gene detection with a gold electrode modified with DNA probes and an electrochemically active dye. *Anal. Chem.* **66,** 3830–3833 (1994).

76. Fojta, M. & Palecek, E. Supercoiled DNA-modified mercury electrode: A highly sensitive tool for the detection of DNA damage. *Anal. Chim. Acta* **342,** 1–12 (1997).

77. Boon, E. M., Ceres, D. M., Drummond, T. G., Hill, M. G. & Barton, J. K. Mutation detection by electrocatalysis at DNA-modified electrodes. *Nat. Biotechnol.* **18,** 1096–1100 (2000).

78. Fan, C., Plaxco, K. W. & Heeger, A. J. Electrochemical interrogation of conformational changes as a reagentless method for the sequence-specific detection of DNA. *Proc. Natl. Acad. Sci. U. S. A.* **100,** 9134–9137 (2003).

79. Petrovykh, D. Y., Kimura-Suda, H., Whitman, L. J. & Tarlov, M. J. Quantitative analysis and characterization of DNA immobilized on gold. *J. Am. Chem. Soc.* **125,** 5219–5226 (2003).

80. Herne, T. M. & Tarlov, M. J. Characterization of DNA probes immobilized on gold surfaces. *J Am Chem Soc* **119,** 8916–8920 (1997).

81. Su, L., Sankar, C. G., Sen, D. & Yu, H. Z. Kinetics of ion-exchange binding of redox metal cations to thiolate - DNA monolayers on gold. *Anal. Chem.* **76,** 5953–5959 (2004).

82. Miranda, P. B. & Shen, Y. R. Liquid Interfaces: A Study by Sum-Frequency Vibrational Spectroscopy. *J. Phys. Chem. B* **103,** 3292–3307 (1999).

83. Bučková, M. *et al.* Detection of damage to DNA and antioxidative activity of yeast polysaccharides at the DNA-modified screen-printed electrode. *Talanta* **56,** 939–947 (2002).

84. Korbut, O., Bučková, M., Tarapčík, P., Labuda, J. & Gründler, P. Damage to DNA indicated by an electrically heated DNA-modified carbon paste electrode. *J. Electroanal. Chem.* **506,** 143–148 (2001).

85. Ovádeková, R., Jantová, S. & Labuda, J. Detection of the Effective DNA Protection by Quinazolines Using a DNA - Based Electrochemical Biosensor. *Anal. Lett.* **38,** 2625–2638 (2005).

86. Boon, E. M., Salas, J. E. & Barton, J. K. An electrical probe of protein-DNA interactions on DNA-modified surfaces. *Nat. Biotechnol.* **20,** 282–286 (2002).

87. Mabbott, G. a. An introduction to cyclic voltammetry. *J. Chem. Educ.* **60,** 697 (1983).

88. Hirata, Y. & Mataga, N. Monophotonic Ionization from the Vibrationally Unrelaxed Excited Singlet State of N,N,N',N'-Tetramethyl-p-phenylenediamine

in Acetonitrile Solution. *Society* **I,** 3872–3874 (1990).

89. Egdell, R., Green, J. C., & Rao, C. N. R. Photoelectron spectra of substituted benzenes. *Chemical Physics Letters*, **33(3)**, 600-607. (1975).

90. Rosi, N. L. *et al.* Oligonucleotide-modified gold nanoparticles for intracellular gene regulation. *Science* **312,** 1027–1030 (2006).

91. Liu, J. & Lu, Y. A colorimetric lead biosensor using DNAzyme-directed assembly of gold nanoparticles. *J. Am. Chem. Soc.* **125,** 6642–6643 (2003).

92. Liu, J. & Lu, Y. Fast colorimetric sensing of adenosine and cocaine based on a general sensor design involving aptamers and nanoparticles. *Angew. Chemie - Int. Ed.* **45,** 90–94 (2005).

93. Paredes, J. I., Marti, a, Tasco, J. M. D. & Martı, a. Graphene Oxide Dispersions in Organic Solvents Graphene Oxide Dispersions in Organic Solvents. *Langmuir* **24,** 10560–10564 (2008).

94. Oh, Y. J. *et al.* Oxygen functional groups and electrochemical capacitive behavior of incompletely reduced graphene oxides as a thin-film electrode of supercapacitor. *Electrochim. Acta* **116,** 118–128 (2014).

95. Qiu, J. D., Wang, G. C., Liang, R. P., Xia, X. H. & Yu, H. W. Controllable deposition of platinum nanoparticles on graphene as an electrocatalyst for direct methanol fuel cells. *J. Phys. Chem. C* **115,** 15639–15645 (2011).

96. Zhou, Y.-G., Chen, J.-J., Wang, F., Sheng, Z.-H. & Xia, X.-H. A facile approach to the synthesis of highly electroactive Pt nanoparticles on graphene as an anode catalyst for direct methanol fuel cells. *Chem. Commun. (Camb).* **46,** 5951–5953

(2010).

97. Xu, Y. *et al.* A graphene hybrid material covalently functionalized with porphyrin: Synthesis and optical limiting property. *Adv. Mater.* **21,** 1275–1279 (2009).

98. Liu, Y. *et al.* Synthesis, characterization and optical limiting property of covalently oligothiophene-functionalized graphene material. *Carbon N. Y.* **47,** 3113–3121 (2009).